Chapter 4

Synthesis of metallogels of tricopper complex, $[Cu_3(bipy)_3(H_3ins)]X_3$, with carbonate base and their application as heterogeneous catalysts for oxidation of phenols

Chapter 4 Synthesis of metallogels of tricopper complex, $[Cu_3(bipy)_3(H_3ins)]X_3$, with carbonate base and their application as heterogeneous catalysts for oxidation of phenols

4.1 Introduction

The previous chapters give an insight about the synthesis/designing of gels and different factors like temperature, solvent, counter anions as well as non-covalent[1–7] interactions like H-bonding and π-π stacking affecting the gel formation ability and their properties.[8–10] As already been discussed in chapter 1 the gels owing to their properties are used in various fields like sensors,[11–13] drug delivery systems,[5,14,15] tissue-engineering,[16] aerospace,[17] templated nonmaterial synthesis[18] and optoelectronic devices.[19]

Apart from the numerous applications mentioned above, the presence of metal ions/ metal atoms in the structure/ composition of gels widens the already versatile scope of the application of these gels. Metallogels are the gels that have a presence of a metal as an integral part in the framework or the structure of the gels. Owing to the presence of metal ions/atoms in the metallogels many of the unusual properties like catalytic activity,[20–22] redox responsive,[23,24] stimuli responsive,[25,26] photoemissive,[25,27,28] magneto-optical switching properties[29] are exhibited by metallogels.

The reversible nature of the supramolecular assembly could give rise to tunable catalytic property. The supramolecular assemblies can also be used as catalytic support materials. Amongst the advantages mentioned above, the supramolecular gelator systems being semi-solid can be filtered, dried and reused. The semi-solid systems can also be separated from the liquid phase/solvent by simply decanting the solvent present over the layer of gels, thus simplifying their separation from the products.

In the last decade there has been an increase in the reports where supramolecular gelator systems have been used as catalysts.

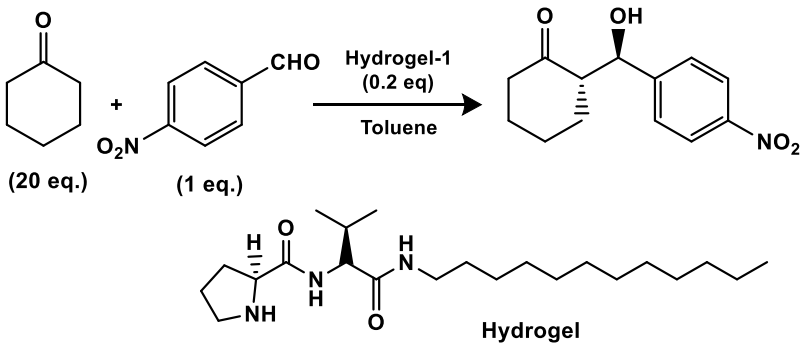

Scheme 4.3.1 Aldol reaction between p-nitrobenzaldehyde and cyclohexanone catalyzed using the hydrogel (Escuder *et al*[30]).

Among the many catalytic reactions reported using gels as catalyst aldol condensation reaction is the most studied one **(Scheme 4.3.1)**. B. Escuder *et al*[30] reported the aldol reaction between p-nitrobenzaldehyde and cyclohexanone where the amphiphilic peptide ProValC_{12} was used as gelator to obtain hydrogel at 2 mM.[30]

In another report a low molecular weight hydrogelator with covalently appended imidazole moiety behaved as an efficient catalyst showing Michaelis-Menten type kinetics. The assembly was reported to hydrolyse p-nitrophenyl acetate (pNPA) as well as inactivated esters, L- and D-phenylalanine methyl esters. [31]

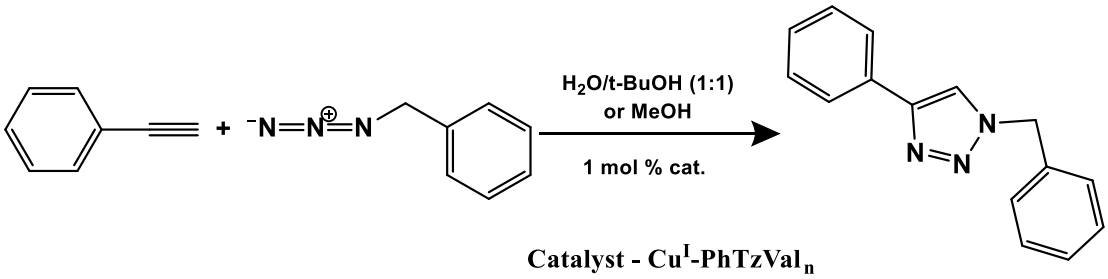

Scheme 4.3.2 Huisgen 1,3-dipolar cycloaddition between phenylacetylene and benzylazide in presence of the L-valine derived gelator as a catalyst (Estuder *et al*[32]).

Escuder *et al*[32] reported the use of copper(I) metallohydrogel functionalized with a phenyltriazole fragment formed in methanol by L-valine derived gelators $(PhTzVal)_2C_n$ for multicomponent aldol-'click' reactions **(Scheme 4.3.2)**. It was used as heterogeneous catalyst for the azide-alkyne cycloaddition between phenylacetylene and benzylazide, as well as for the autocatalytic synthesis of the gelator itself.[32]

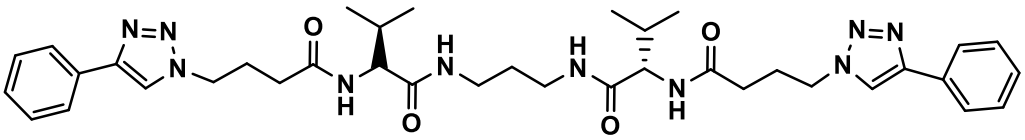

Figure 4.3.1 Structure of the gelator of **$PhTzVal_3$ (Estuder *et al*[33])**.

Escuder *et al*[33] reported a tandem aldol-click reaction between phenylacetylene, p-nitrobenzaldehyde, and an azide containing a ketone moiety. The reaction was performed using hydrogels formed by the L-valine gelator **(Figure 4.3.1)** in presence of Cu(I)[33] as a catalyst.

Huisgen 1,3 dipolar cycloaddition between phenylacetylene and benzylazide reported was also reported by Escuder *et al*[33] using Cu(I) metallogels formed by L-valine amphiphilic gelator, $CrTzValC_{12}$, with only one triazole functionality.[34]

Emphasizing on the fact that metallogels can prove out to be efficient catalyst, click reactions were carried out using several substrates using supramolecular gels formed by glycoclusters with three, four, and six arms of glycosyl triazoles in presence of $CuSO_4$. Gel columns were prepared and they were found to be more efficient than the corresponding solutions. These gel columns could also be reused.[35]

In another one such report copper(II) based metallogels were used as a reaction media for Diels-Alder cycloaddition between cyclopentadiene and azachalcone.[36]

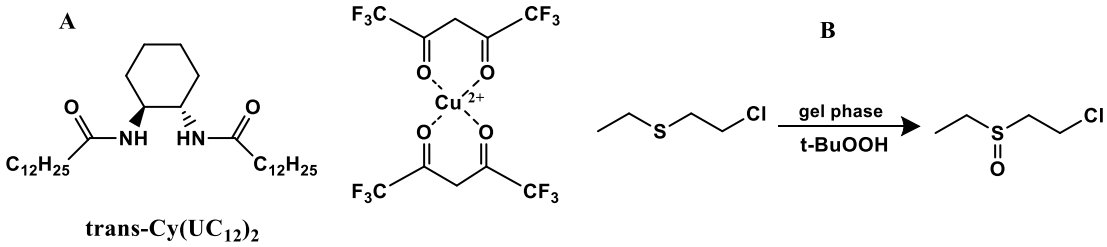

Figure 4.3.2 Figure (A) showing the structure of organogelator and copper(II) complex and (B) schematic representation of oxidation of model sulfur mustard compound (Hiscock *et al)*[37].

Oxidation of sulphur mustard compound (**Figure 4.3.2)** was achieved using copper(II)-doped organogels formed by a urea-based gelator as catalysts. Sulfur mustards are vesicant halogenated sulfide species, potentially used as chemical warfare agents. The oxidation of such compounds to their sulfoxides is necessary for the decontamination of soils and the neutralization of such compounds. In order to carry out the oxidation of a sulfur mustard model compound, Hiscock *et al.*[37] used an organogel of bis-urea doped, *trans*-Cy$(UC_{12})_2$, with a complex of copper(II) with hexafluoroacetylacetonate, Cu$(hfac)_2$, in the presence of *tert*-butyl hydroperoxide (*t*-BuOOH).[37]

Copper(II) is known for its oxidative activity. Hence, the metallogels containing copper(II) can be exploited as oxidation catalysts due to this property. Sarkar *et al* have reported the formation of a metallogel containing cupric chloride along with 2 ligands disodium succinate and hexamethylenetetramine. The metallogel thus formed was used as a heterogeneous catalyst for oxidative conversion of 2-aminophenol (OAPH) to phenoxazinone using atmospheric oxygen and thereby conferring its role as a biomimetic nanozyme catalyst.[38]

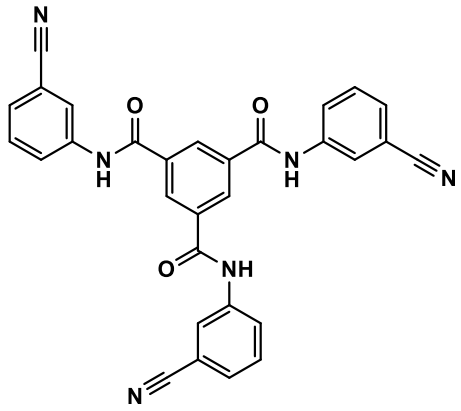

Figure 4.3.3 Figure showing the gelator molecule used for catalysis reaction of catechols.

Copper(II) metallogel reported by Mukhopadhyay *et. al.* was used as both, catalyst and reaction medium itself, for aerobic oxidation of catechols to quinones. The structure of the gelator molecule is shown in the **Figure 4.3.3.**[39]

A supramolecular assembly resulting from the trinuclear copper (II) complex of myo-inositol(ins) and 2,2'-bipyridine(bipy), **[$Cu_3(H_3ins)(bipy)_3$]X_3**, in which X was varied as $HCOO^-$, CH_3COO^- and $CH_3CH_2COO^-$ were discussed and have been mentioned in chapter 2. These gels, however, were formed at a pH of 12.4 which is highly alkaline. This restricts the biological applications of the metallogels. The primary aim was to reduce the pH at which gelation takes places. The same was achieved by forming the trinuclear copper (II) complex of myo-inositol(ins) and 2,2'-bipyridine(bipy), **[$Cu_3(H_3ins)(bipy)_3$]X_3**, where X = $HCOO^-$, CH_3COO^- and $CH_3CH_2COO^-$ in presence of carbonate base at pH of 8.5-9 which has been mentioned in the current chapter.

The metallogels were characterized using, UV-Vis spectroscopy, FT-IR, SEM and ESI-MS analysis. The supramolecular assembly resulting in the formation of the metallogels which are discussed in the current chapter are formed by a trinuclear coordination complex involving copper(II) at its center. Since copper(II) systems are widely known to participate in oxidase activity, similar activity was carried out with the metallogels. The rigidity of the metallogels makes them behave as heterogeneous catalysts which facilitates easy and efficient transfer of the products once formed. The current work involving oxidase activity with different substrates has been further discussed in this chapter.

4.2 Experimental Section

4.2.1 Materials

Copper(II) acetate monohydrate, 2,2'-bipyridine (bipy), were purchased from Qualigens, myo-inositol (ins) from Sigma-Aldrich, K_2CO_3 and Na_2CO_3 from Qualigens. All the chemicals were of AR or GR grade and were used for synthesis without further purification. Copper(II) dihydrate and copper(II) propionate were prepared by reacting formic acid and propionic acid with cupric carbonate, respectively. Reagent grade cupric carbonate was procured from local manufacturers, formic acid and propionic acid were procured from Merck. These chemicals were also used without further purification. Triple distilled water was used as solvent for the synthesis of gels. Substrates used for oxidation activity like 3,5-di tert-butylcatechol (3,5-DTBC), 4-methyl catechol, 2,3-dihydroxy naphthalene, hydroquinone, resorcinol and pyrocatechol were procured from Sigma-Aldrich. Solvents were procured from spectrochem.

4.2.2 Synthesis

The reaction of myo-inositol with 3 equivalents of copper carboxylate salts and varying amounts of 2,2'-bipyridine (bipy) was carried out. Gel formation was tried by adding varying concentrations of base (K_2CO_3/Na_2CO_3). The reaction of 10 ml 2.5% aqueous solution (1.388 mmol) of myo-inositol was carried out with 3 equivalents of $[Cu(bipy)]^{2+}$ complex obtained by reacting 0.638 g (4.163 mmol) of copper(II) formate dihydrate and 0.650 g (4.163 mmol) of bipy in 25 ml water **(Scheme 4.2.2.1)**. Subsequently the pH was raised to 8.5 with aqueous K_2CO_3. The solution was heated in oven at 75 °C for 120 minutes after which gel formation took place (**132**). Repeating the same procedure with copper(II) acetate monohydrate (0.831 g, 4.163 mmol) and copper(II) propionate (0.8725, 4.163 mmol) resulted in the formation of green transparent gels, **131** and **133**, respectively. The same procedure was repeated using equivalent amounts of all reagents but using aqueous sodium carbonate as base in place of potassium carbonate to get the gels **151**, **152**, **153**, respectively with copper(II) formate, copper(II) acetate and copper(II) propionate. The gelation was confirmed by the inverted test tube method **(Figure 4.2.2.1)**.

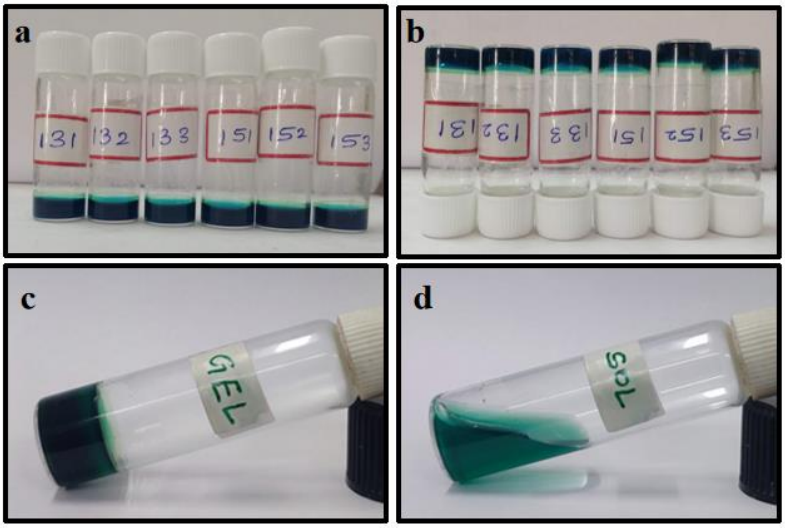

Figure 4.2.2.1 (a) Gels formed by the trinuclear **$[Cu_3(H_3ins)(bipy)_3]^{3+}$** at pH 8.5 in presence of K_2CO_3, (b) Image of inverted vials which proves gel formation, (c) gel-132 and (d) solution of gel -132 showing the sol-gel transformation on thermal stimuli.

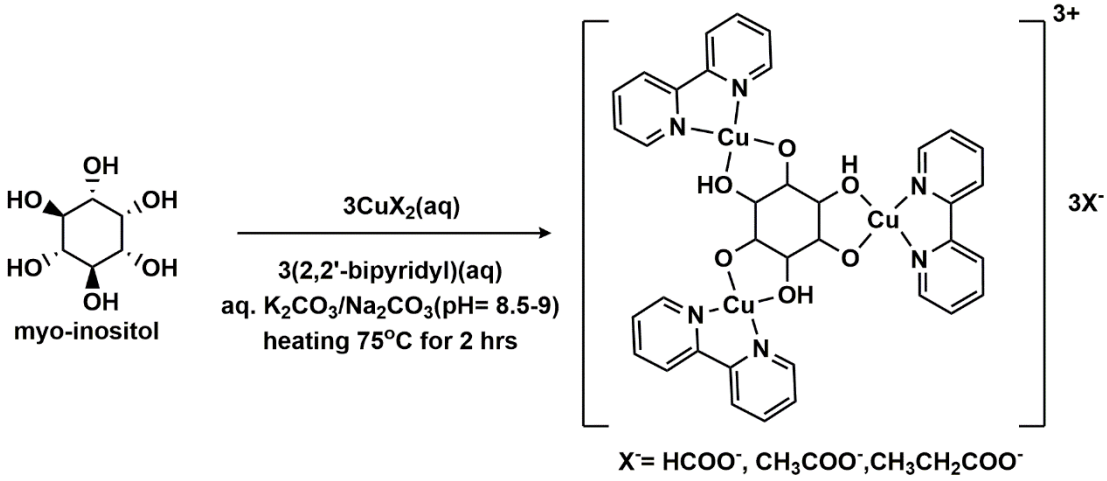

Scheme 4.2.2.1 Scheme showing the synthesis of the metallogelator complex.

4.2.3 Instrumentation and Techniques

UV-Visible: Perkin Elmer Lambda 35 dual beam UV–vis Spectrophotometer was used to record the spectra of metallogels as well as for monitoring the extent of reaction/ amount of oxidation of substrate formed during the catalytic reactions.

T_{gel}: T_{gel} of the gels were measured using Julabo 5A thermostat with a temperature controller and thermometer with an accuracy of ± 0.05 °C. Gels were taken in a screw capped glass vial and immersed in a water bath whose temperature was gradually increased by a temperature control program and the T_{gel} temperature of the gels was recorded by inverted test-tube method.

FTIR: FT-IR spectra of the xerogels were recorded using PerkinElmer (Model: RX1) and Bruker Alpha FT-IR spectrometer in solid state as KBr pellets.

Mass spectrometry: The ESI mass spectra of the hydrogels were recorded using Applied Biosystem API 200 mass spectrometer.

Scanning electron microscopy (SEM): SEM analysis was performed using JEOL JSM-5610 instrument. Xerogels were prepared on SEM stubs for capturing the SEM images.

Polarizing optical microscopy: POM analysis was performed using LEICADM2500P polarizing microscope. Images were captured using LEICADFC295 camera which is attached with the instrument. Images were processed used a software LAS V4.1. A thin layer of gel was formed on a glass slide and allowed to dry and get converted to a xerogel whose images were captured at various magnifications and different angles of polarizer.

ESR: ESR of the metallogelator complexes were recorded using E-112 VARIAN USA spectrometer in solution phase (H_2O) at RT using X- band frequency (9.45 GHz).

4.3 Results and Discussion

4.3.1 UV-Visible spectroscopy

As discussed previously **(Scheme 4.2.2.1)**, the trinuclear copper(II) complex is formed by reaction of copper salts with 2,2'-bipyridine and myo-inositol in presence of carbonate bases like K_2CO_3 and Na_2CO_3. The supramolecular assembly is formed by the trinuclear copper complex **$[Cu_3(H_3ins)(bipy)_3]^{3+}$**. The ternary complex along with the carbonate anion led to the formation of a supramolecular assembly resulting in a metallogel. The change in the coordination sphere of metal center was confirmed by UV-Visible spectroscopy (**Figure 4.3.1.1)**. It was seen that there is a shift in the λ_{max} **(Table 4.3.1.1)** and a transition in colour from a blue-coloured gel forming copper complex to a green-coloured gel. The shift was observed in case of all 3 gels **131**, **132** and **133**. In the metallogels reported here the copper(II) center is coordinated to 2,2'-bipyridine and myo-inositol. The metallogels are formed owing to the presence of trinuclear copper complex and the carbonate anion, which leads to the formation of stacks resulting in the formation of a supramolecular assembly. The

shift in the λ_{max} is a result of a change in the coordination sphere of the metal center on the formation of supramolecular assembly, indicating that these are two component gels. The shift in the λ_{max} values recorded using UV-Visible spectroscopy can be clearly seen in the **Figure 4.3.1.1.**

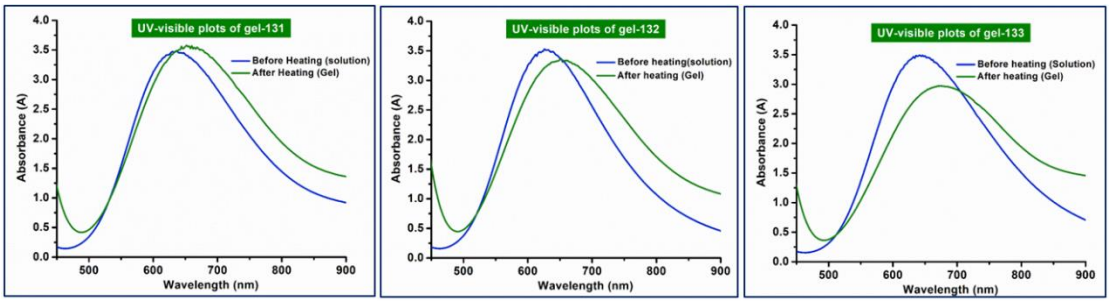

Figure 4.3.1.1 The UV-visible spectra of metallogels **131, 132** and **133**.

The change in the λ_{max} values for the three metallogels have been summarized in **Table 4.3.1.1** along with the ε_{max} (Molar absorptivity coefficient) values.

Table 4.3.1.1 The λ_{max} and ε values of the metallogels

Codes	λ_{max} (nm)	ε -Molar absorptivity coefficient ($M^{-1}cm^{-1}$)
131-solution	**636**	**219.66**
131-gel	**652**	**225**
132-solution	**626**	**206.07**
132-gel	**650**	**196.03**
133-solution	**642**	**259**
133-gel	**674**	**237**

4.3.2 Sol-Gel Transition temperature (T_{gel})

The metallogels reported in this chapter are susceptible to thermal changes. The characteristic T_{gel} temperatures were recorded for all these gels by inverted vial experiments **(Table 4.3.2.1)**.

The metallogels as mentioned in the **Scheme 4.2.2.1** were synthesized in presence of Na_2CO_3 or K_2CO_3 as a base, the counter anions which are alkyl carboxylates were also varied.

Though the cation, i.e., sodium or potassium, in the carbonate bases used for maintaining the pH is not a part of the assembly and is present to balance the charges only, seems to have a significant effect on the pH of the gels. The gels prepared using

Na_2CO_3 as a base have significantly higher T_{gel} values than the gels prepared using K_2CO_3. The carboxylate anions also have a significant effect on the gel properties. This can be seen in a gradual decrease in the T_{gel} values. The T_{gel} gradually decreases as the alkyl chain of the counter anion increases from formate to acetate to propionate in the corresponding gels.

Table 4.3.2.1 Codes and T_{gel} values of the metallohydrogels

Code	Counter Anion	Base	T_{gel} (°C)
131	Formate	K_2CO_3	**77**
132	Acetate	K_2CO_3	**47**
133	Propionate	K_2CO_3	**44**
151	Formate	Na_2CO_3	**88**
152	Acetate	Na_2CO_3	**55**
153	Propionate	Na_2CO_3	**51**

4.3.3 FT-IR Spectroscopy

The metallo-hydrogels formed by the trinuclear copper(II) complexes were dried and converted to xerogels in order to record their FTIR spectra. The FTIR spectra (KBr) of xerogels exhibited important stretchings of both myo-inositol and bipy. Among these the aliphatic C-H stretching vibrations at 2700-3000 cm^{-1}, the C-C multiple bond stretching and the ring C-N vibration in bipy between 1400-1700 cm^{-1} were prominent. The presence of absorptions at ~1030, 900 and 770 cm^{-1} supported the coordination of bipy while the absorptions at ~1100, 730 and 660 cm^{-1} supported the presence of coordinated inositol **(Figure 4.3.3.1 to Figure 4.3.3.6)**. The xerogels were washed with ethanol followed by water to remove free bipy, copper acetate and binary complexes, if, any formed during the reaction as these were freely soluble. Thus, the residue obtained after washing was expected to be the corresponding ternary complex **$[Cu_3(H_3ins)(bipy)_3]^{3+}$**. As the ternary complex present in the xerogel remained the same, the FT-IR spectra of the xerogels resemble with each other and showed the prominent vibrations as discussed above. As the counter anions were varied during the study the vibrations corresponding to the counter anions namely formate, acetate and propionate were different amongst the xerogels.

FT-IR data for xerogel 131: FT-IR, cm^{-1} (KBr): 3418.32, 2817.27, 1662.17, 1600.09, 1493.77, 1471.34, 1446.35, 1379.95, 1156.33, 1111.32, 1029.79, 952.53, 896.36, 775.95, 731.84, 541.16 **(Figure 4.3.3.1)**

FT-IR data for xerogel 132: FT-IR, cm^{-1} (KBr): 3421.99, 1667.49, 1565.17, 1411.07, 1344.18, 1293.52, 1020.29, 776.00, 652.68 **(Figure 4.3.3.2)**

FT-IR data for xerogel 133: FT-IR, cm^{-1} (KBr): 3417.65, 3079.57, 3031.99, 2870.18, 1649.19, 1602.31, 1496.21, 1472.05, 1447.37, 1381.60, 1357.99, 1314.52, 1293.83, 1202.09, 1157.12, 1110.67, 1029.28, 952.62, 895.87, 779.72, 730.74, 684.97, 662.48, 641.01, 581.85, 544.46, 485.21, 415.29 **(Figure 4.3.3.3)**

FT-IR data for xerogel 151: 3431.76, 2924.90, 2850.91, 2717.81, 1697.54, 1601.86, 1445.24, 1351.63, 1161.85, 1107.40, 1027.57, 951.85, 897.41, 844.93, 774.87, 730.23, 588.71, 514.80, 410.31**(Figure 4.3.3.4)**

FT-IR data for xerogel 152: FT-IR, cm^{-1} (KBr): 3493.82, 3407.77, 3292.18, 3104.83, 3063.59, 3026.37, 2921.68, 1577.12, 1496.00, 1473.73, 1400.56, 1316.05, 1246.97, 1179.85, 1158.90, 1105.48, 1022.42, 922.31, 771.43, 732.04, 675.61, 624.31, 578.16, 509.86, 415.70 **(Figure 4.3.3.5)**

FT-IR data for xerogel 153: FT-IR, cm^{-1} (KBr): 3432.73, 2973.67, 2938.45, 2873.98, 1655.08, 1561.11, 1466.66, 1427.87, 1369.53, 1332.43, 1296.17, 1161.68, 1075.92, 1028.20, 1005.90, 880.31, 815.79, 775.73, 730.19, 645.32, 509.59, 460.74, 431.22, 406.98 **(Figure 4.3.3.6)**

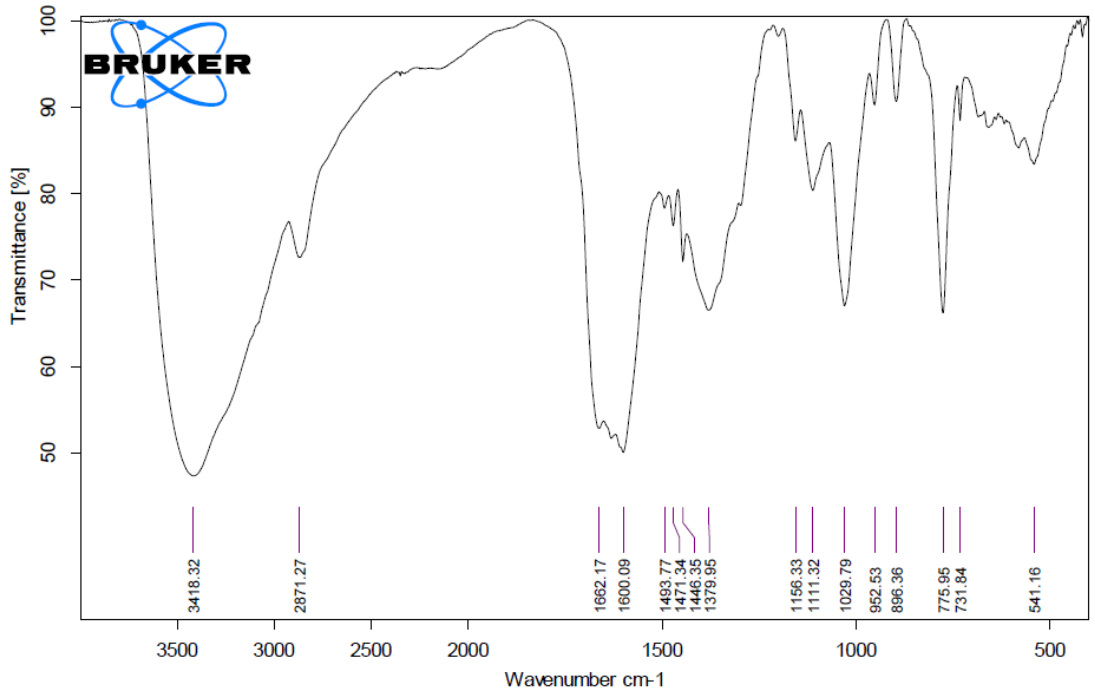

Figure 4.3.3.1 FT-IR spectrum of xerogel **131.**

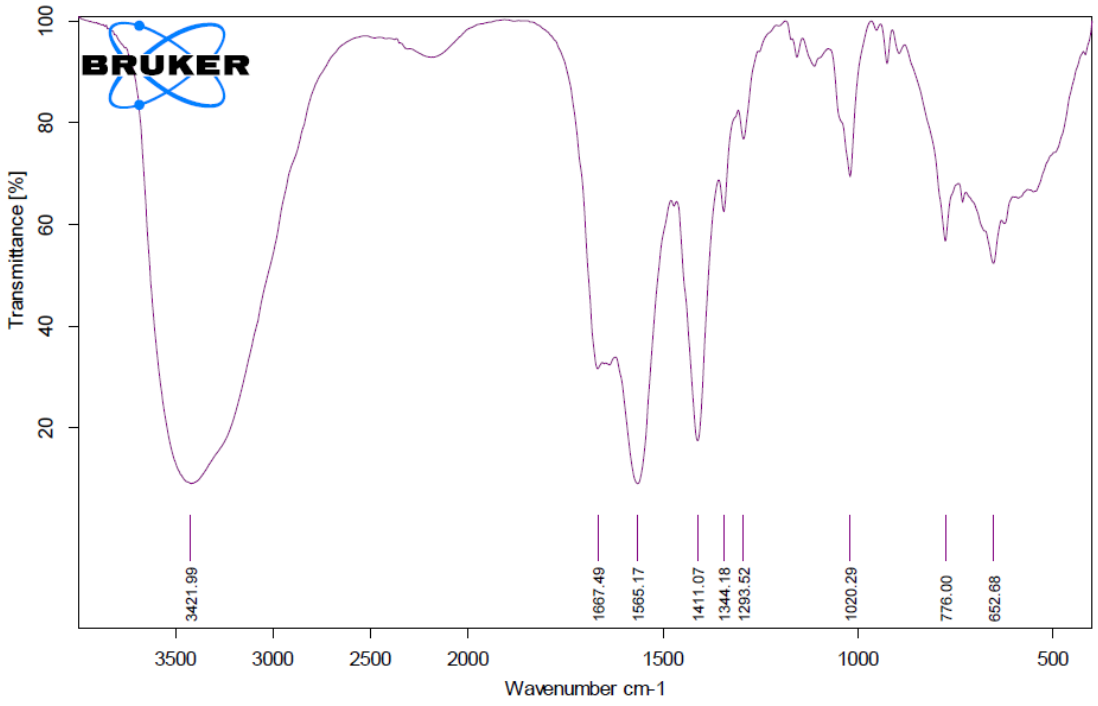

Figure 4.3.3.2 FT-IR spectrum of xerogel **132.**

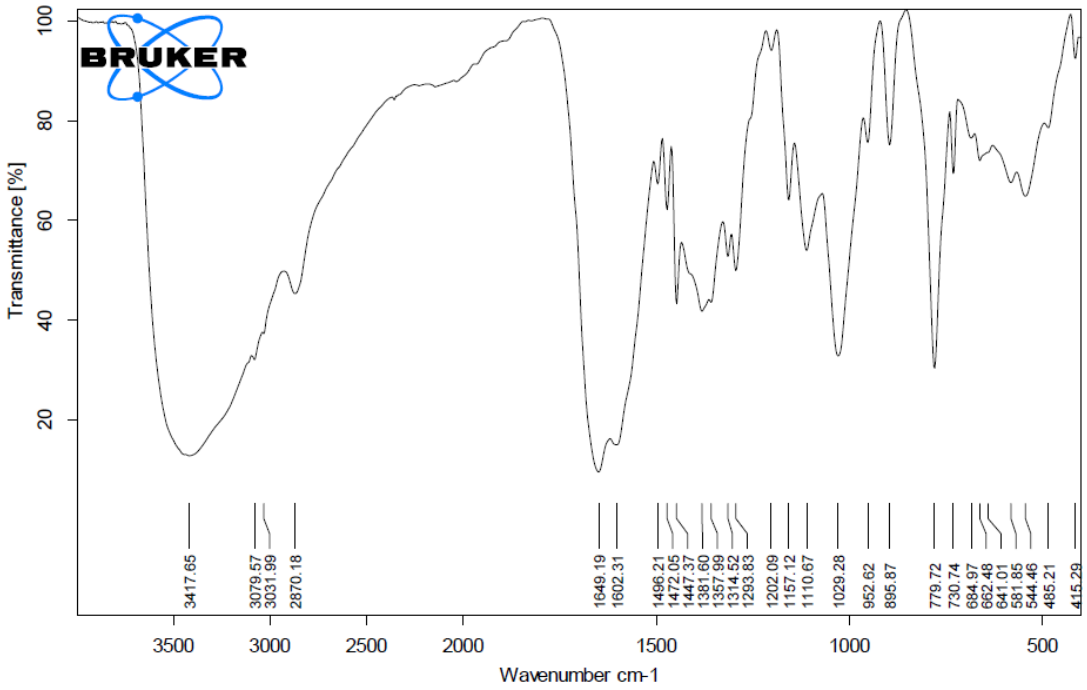

Figure 4.3.3.3 FT-IR spectrum of xerogel **133.**

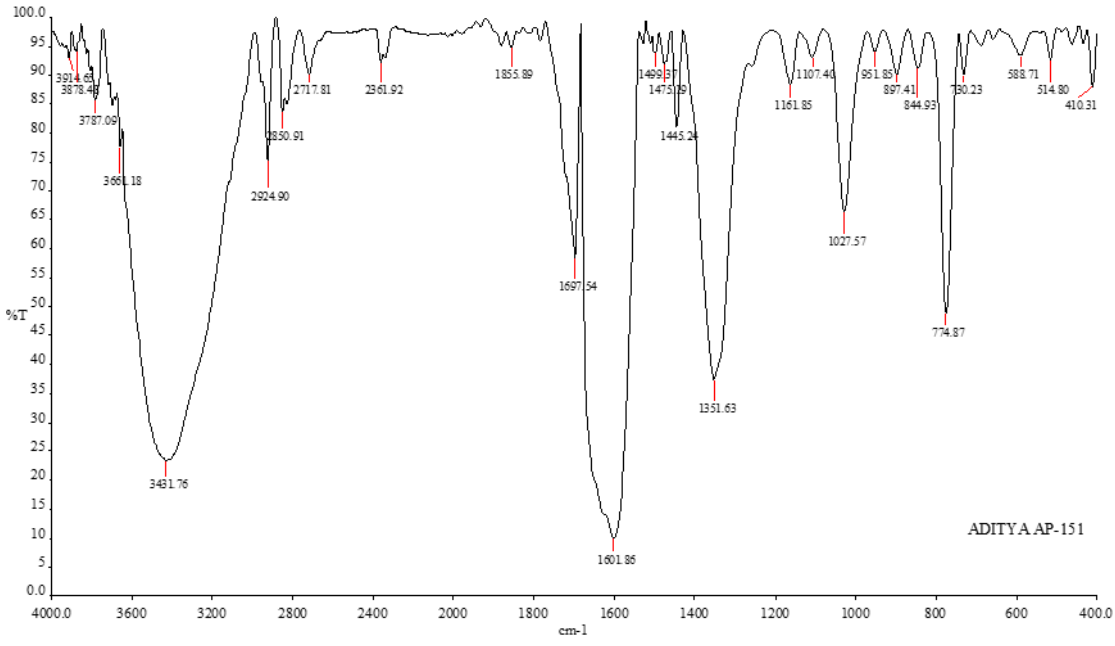

Figure 4.3.3.4 FT-IR spectrum of xerogel **151.**

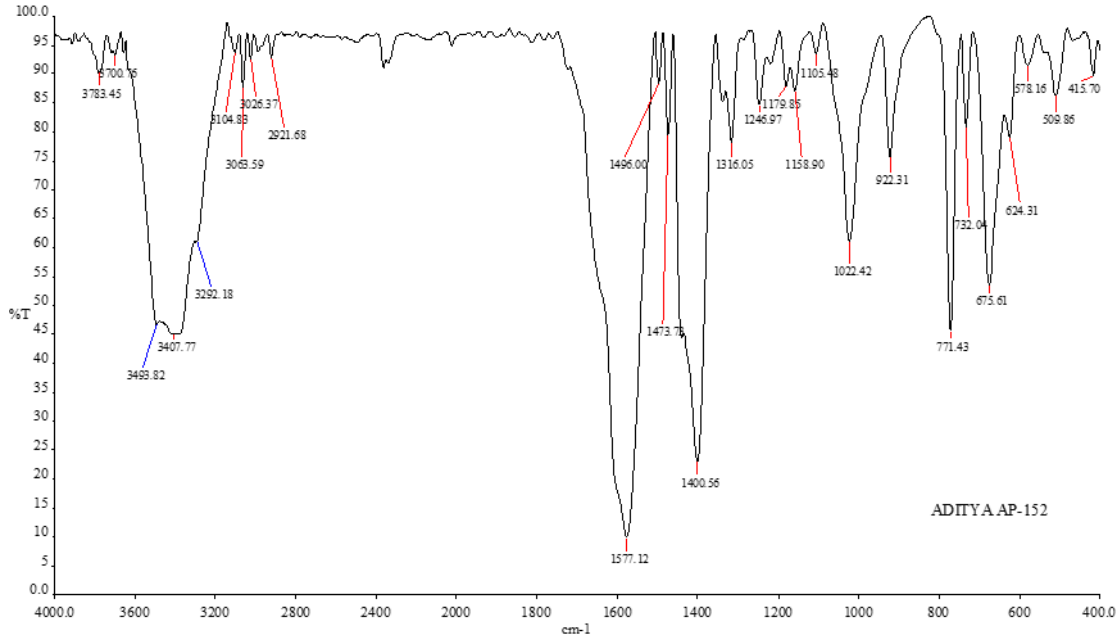

Figure 4.3.3.5 FT-IR spectrum of xerogel **152.**

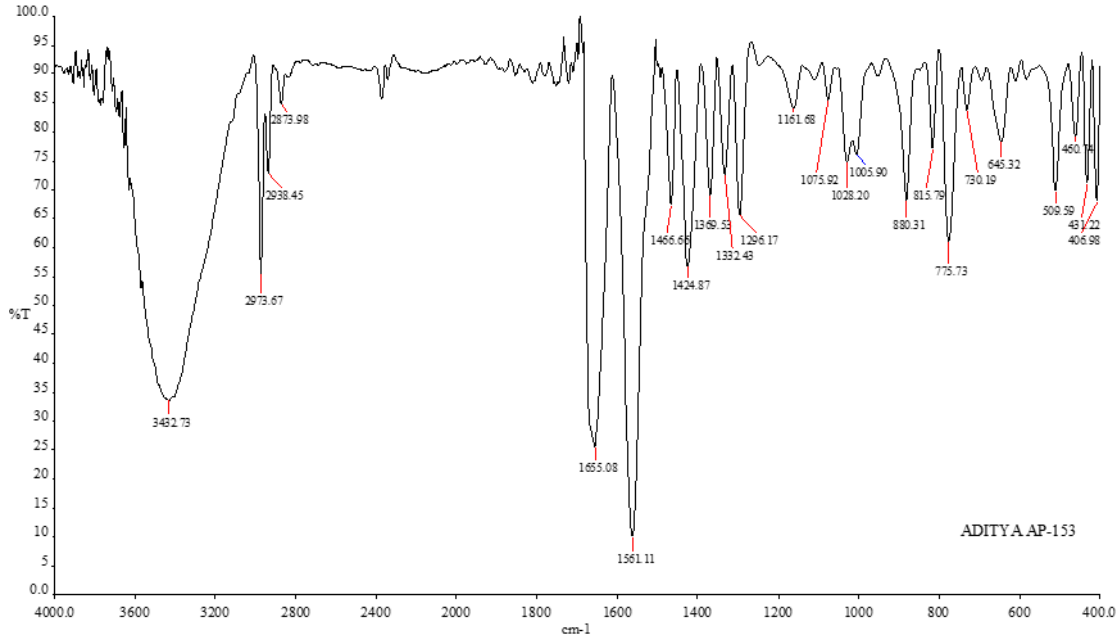

Figure 4.3.3.6 FT-IR spectrum of xerogel **153.**

4.3.4 ESI-MS Analysis of Metallogels

The gels were formed using copper salts and 2,2'-bipyridine (bipy) and myo-inositol as ligands in presence of carbonate bases like potassium carbonate and sodium carbonate. The supramolecular assemblies which result in the formation of the metallogels are formed because of the complex cation **$[Cu_3(H_3ins)(bipy)_3]^{3+}$**. In order to prove the existence of the complex ESI-MS spectroscopy of the metallogels was carried out. The ESI-MS of the gels **(Figure 4.3.4.1 to Figure 4.3.4.6)** recorded in aqueous media has prominent peaks corresponding to $[Cu(bipy)]^{2+}$ (m/z 218.95, 220.9) and $[Cu_3(H_3ins)(bipy)_3]^{3+}$ (m/z=277.95, 279.95). These are related to the isotopic abundance of copper with mass numbers 63 and 65 in 3:1 ratio. The peaks at m/z=277.95, 279.95 have been observed in the mass spectra of all gels. This supports the existence of trinuclear trication, $[Cu_3(H_3ins)(bipy)_3]^{3+}$, in the gels. This trication must be assembling with carbonate anions and further undergoing H-bond formation or coordination with water molecules resulting in the formation of metallogels.

The six gels reported in this chapter very in the counter anions, X^- as formate, acetate or propionate, and the alkali cation Na^+ or K^+ used in the form of carbonate base as K_2CO_3 and Na_2CO_3, the trinuclear trication, $[Cu_3(H_3ins)(bipy)_3]^{3+}$ responsible for the formation of metallogels remained same in all the metallogels. The peaks m/z=277.95, 279.95 which correspond to the trinuclear trication, $[Cu_3(H_3ins)(bipy)_3]^{3+}$ were observed in the mass spectra of all six metallogels **(Figure 4.3.4.1 to Figure 4.3.4.6)**.

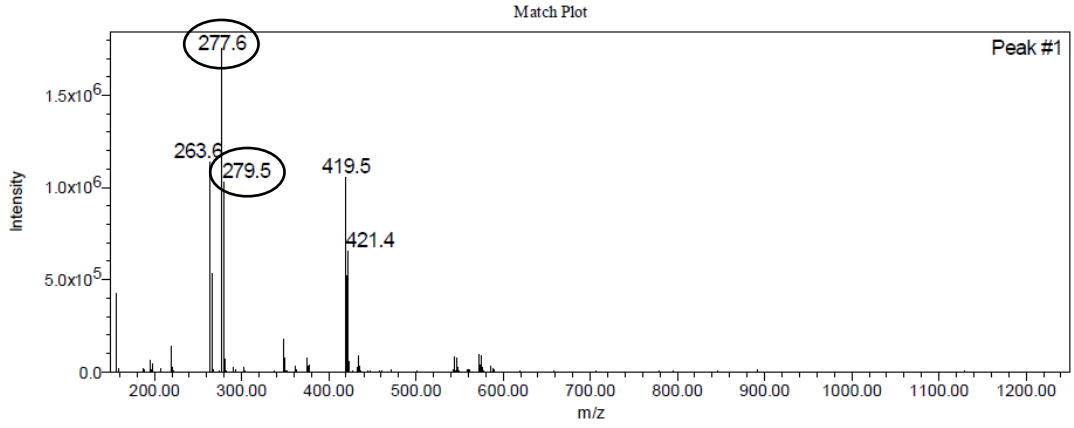

Figure 4.3.4.1 ESI-MS of the metallogel-**131**.

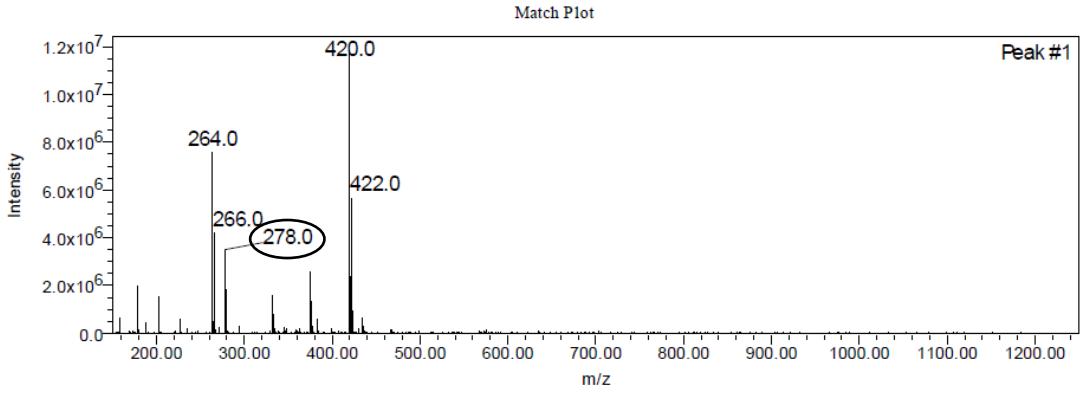

Figure 4.3.4.2 ESI-MS of the metallogel-**132**.

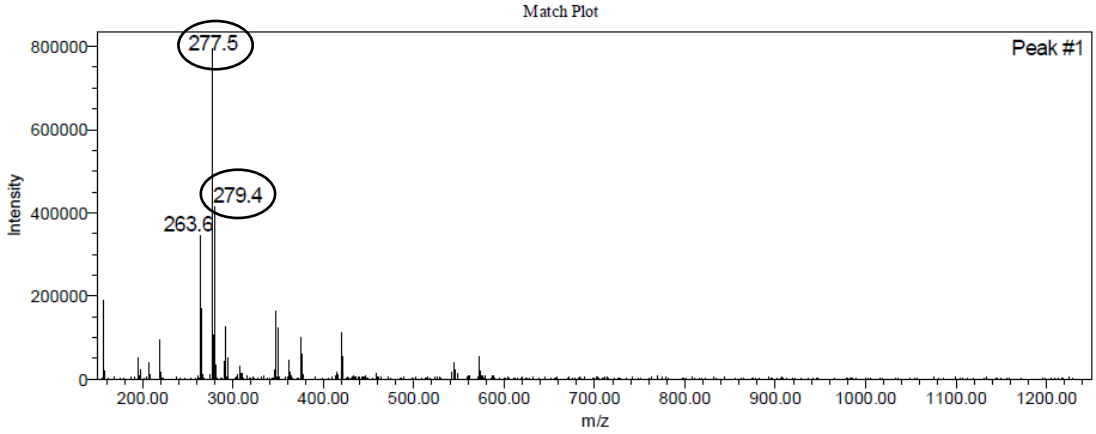

Figure 4.3.4.3 ESI-MS of the metallogel-**133**.

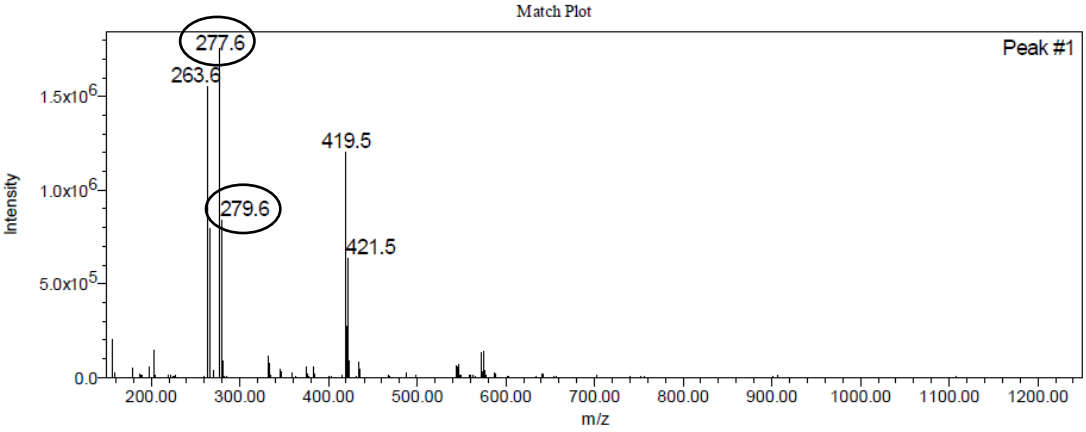

Figure 4.3.4.4 ESI-MS of the metallogel-**151**.

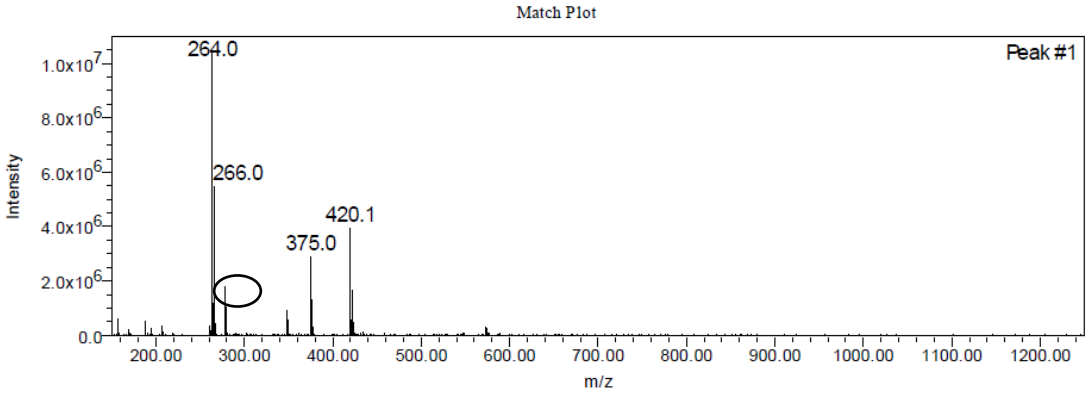

Figure 4. 3.4.5 ESI-MS of the metallogel-**152**.

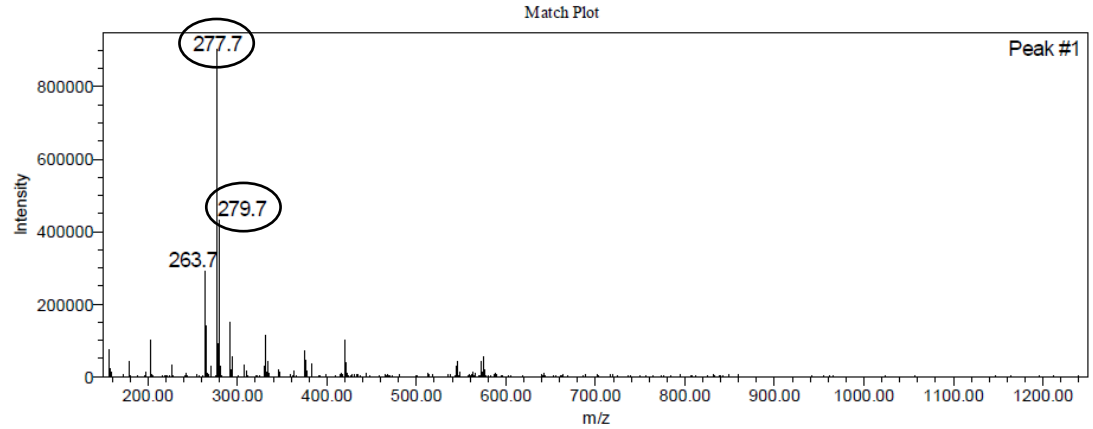

Figure 4.3.4.6 ESI-MS of the metallogel-**153**.

4.3.5 Microscopic Properties

Polarizing Optical Microscopy (POM)

The gel forming complex, being trinuclear has to be dissymmetric having at the most a C_3 symmetry axis. This can induce chirality in the molecule which can further get enhanced by the stacking of molecules and the formation of supramolecular assembly and thus can attribute birefringent property to the gels. As discussed in chapter 2, the metallogels reported in this chapter also showed similar birefringent properties in presence of the polarizing light in microscopic studies.

The POM images of the gels were recorded after drying the metallogels and converting them into xerogels. The POM images captured at various magnifications **(Figure 4.3.5.1 to 4.3.5.6)** show that the assembly is very highly organized and has behavior like columnar lyotropic[40] or more like smectic thermotropic liquid crystalline phases. As the assembly in gels was captured in the form of xerogel by slow evaporation at low to ambient temperatures, the gels can be called as behaving like lyotropic liquid crystalline phases though the term is not very appropriate.

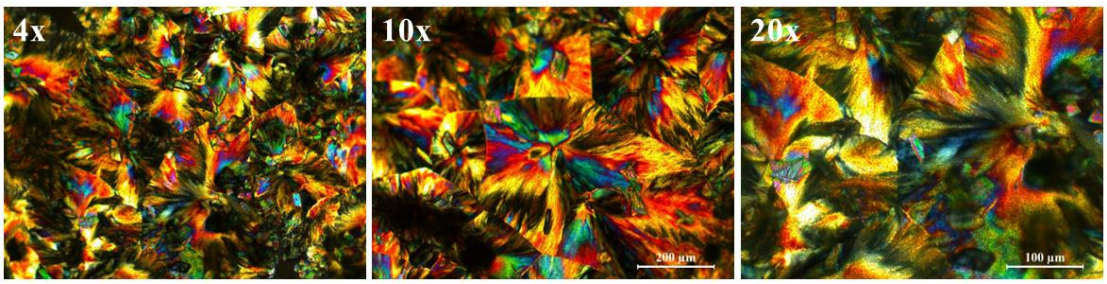

Figure 4.3.5.1 POM images of xerogel **132** at different magnifications **(4x,10x,20x)**.

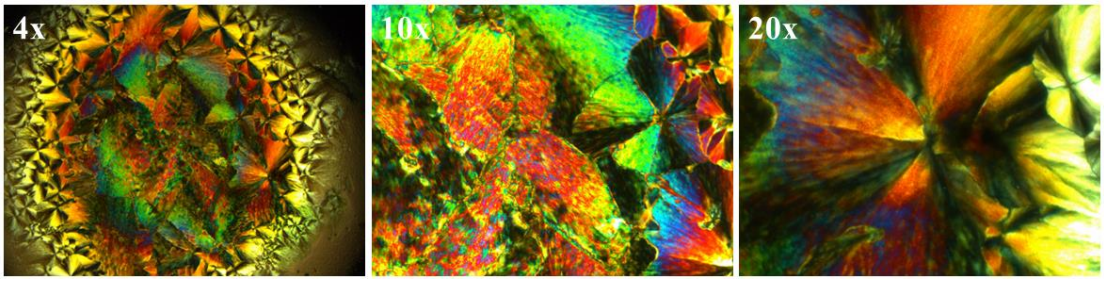

Figure 4.3.5.2 POM images of xerogel **133** at different magnifications **(4x,10x,20x)**.

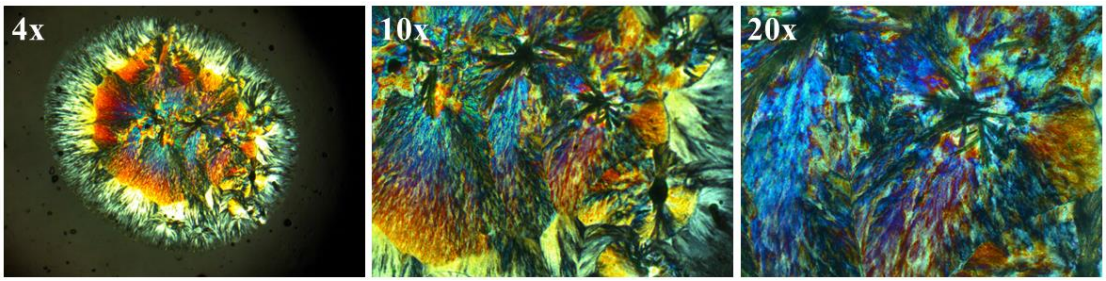

Figure 4.3.5.3 POM images of xerogel **151** at different magnifications **(4x,10x,20x)**.

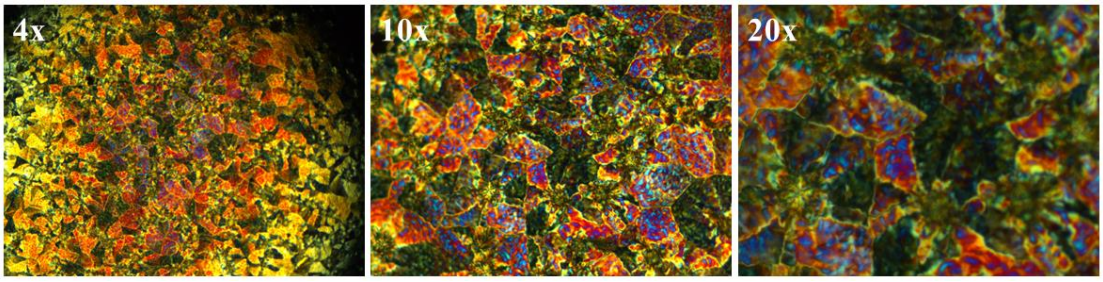

Figure 4.3.5.4 POM images of xerogel **152** at different magnifications **(4x,10x,20x)**.

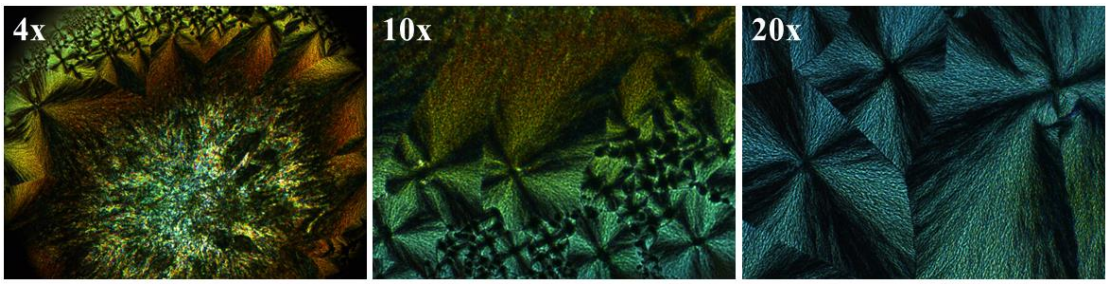

Figure 4.3.5.5 POM images of xerogel **153** at different magnifications **(4x,10x,20x)**.

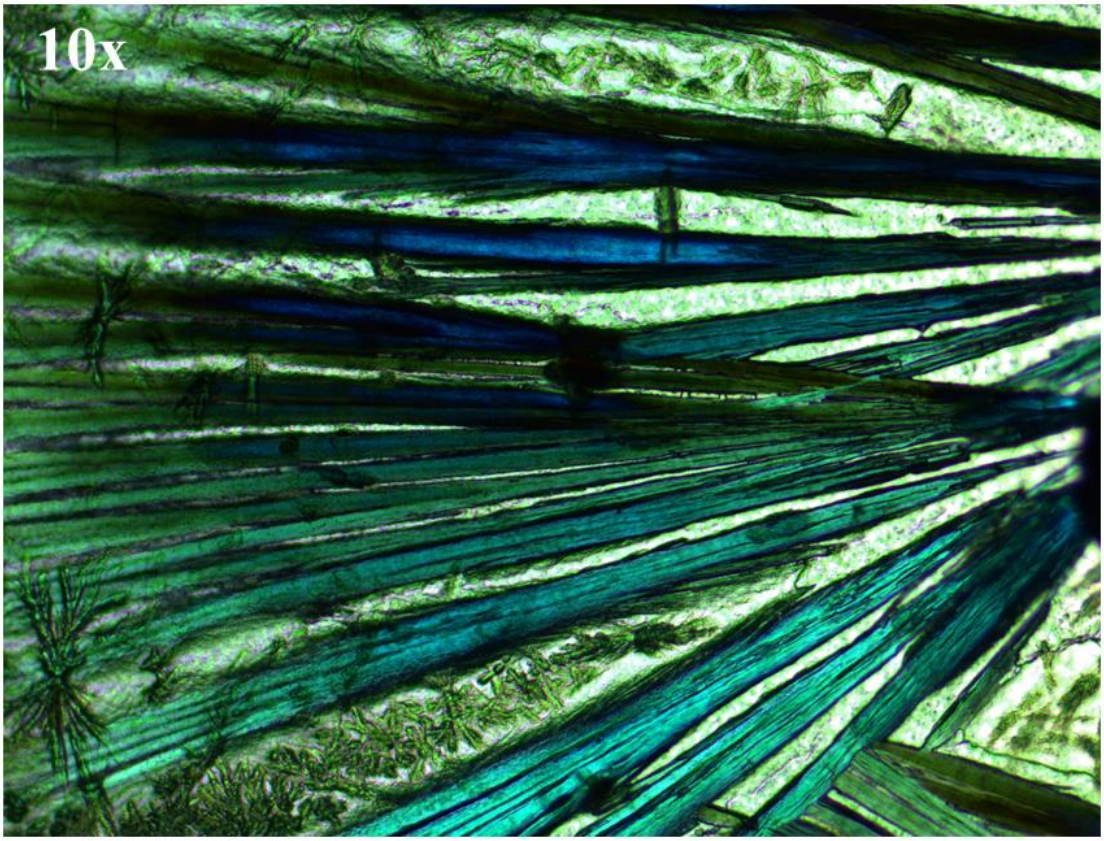

Figure 4.3.5.6 POM image of xerogel **131** at **10x** magnification.

Birefringent properties of metallogels

As discussed previously that since the gelator complex ion has C_3 symmetry and the anisotropy resulting from the C_3 symmetry in the supramolecular assembly leading to birefringence was explored at different angles of polarizer and analyzer using POM. One of the characteristic properties of birefringent materials is that the respond to the change in the angle between polarizer and the analyzer. The images were captured at different angles of the polarizer and the analyzer **(0, 45, 90, 135).** It was observed from the images recorded at different angles of polarizer that the assembly is highly birefringent, such behavior of the gels discussed in the present chapter is unique **(Figure 4.3.5.7 to Figure 4.3.5.12).**

The patterns observed in the POM images also depend on the nature of the counter anions. Thus, these counter anions appeared to have significant effect on the supramolecular assembly.

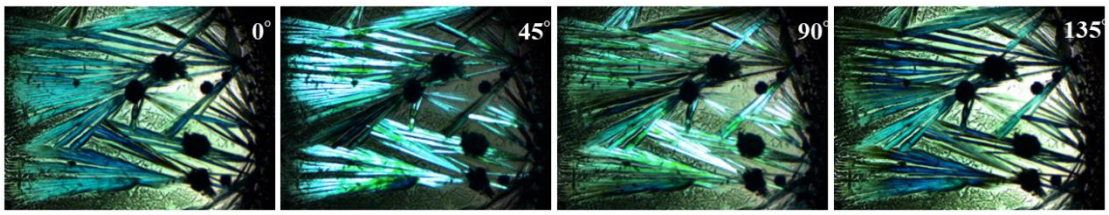

Figure 4.3.5.7 Birefringence and angle dependent POM images of xerogel **131**. **(0, 45, 90, 135)** written after the gel codes on the top right corner in the images represent the angles of polarizer in degrees).

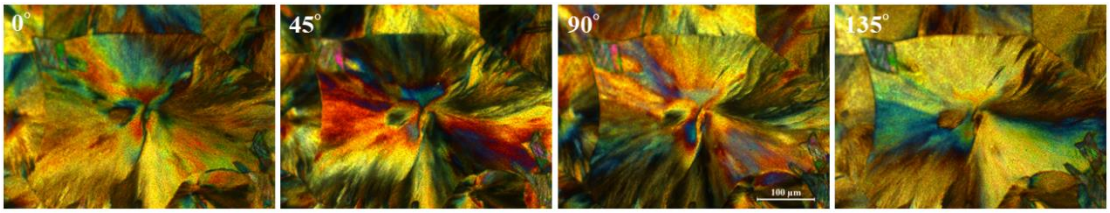

Figure 4.3.5.8 Birefringence and angle dependent POM images of xerogel **132**. **(0, 45, 90, 135)** written after the gel codes on the top right corner in the images represent the angles of polarizer in degrees).

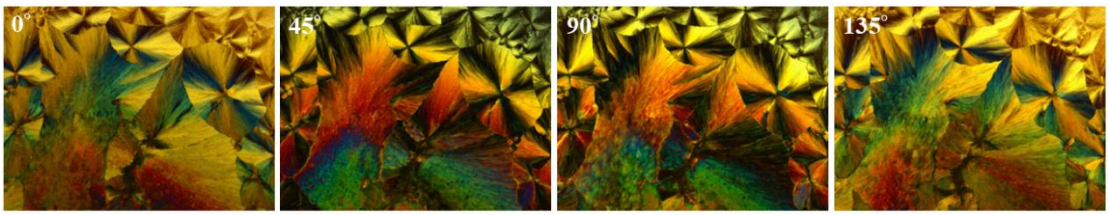

Figure 4.3.5.9 Birefringence and angle dependent POM images of xerogel **133**. **(0, 45, 90, 135)** written after the gel codes on the top right corner in the images represent the angles of polarizer in degrees).

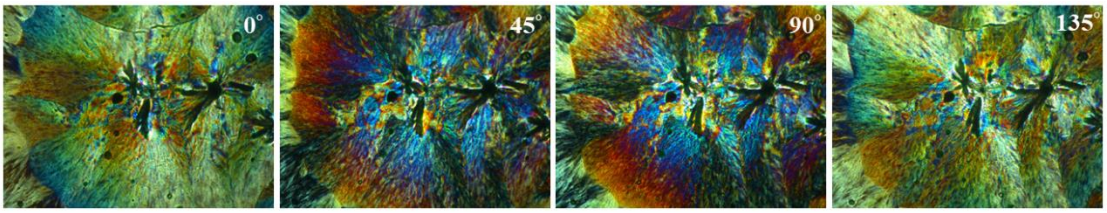

Figure 4.3.5.10 Birefringence and angle dependent POM images of xerogel **151**. **(0, 45, 90, 135)** written after the gel codes on the top right corner in the images represent the angles of polarizer in degrees).

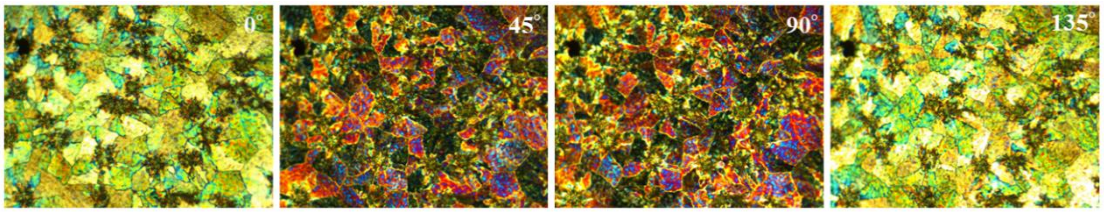

Figure 4.3.5.11 Birefringence and angle dependent POM images of xerogel **152**. **(0, 45, 90, 135)** written after the gel codes on the top right corner in the images represent the angles of polarizer in degrees).

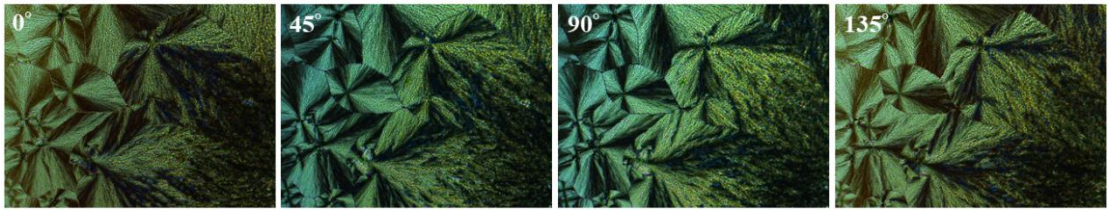

Figure 4.3.5.12 Birefringence and angle dependent POM images of xerogel **153**. **(0, 45, 90, 135)** written after the gel codes on the top right corner in the images represent the angles of polarizer in degrees).

Scanning Electron Microscopy of metallogels (SEM)

The trinuclear copper(II) complex discussed in this chapter previously was responsible for the formation of metallogel. The gels are formed because of the fibrous assembly. In order to get an insight in the morphology of the metallogels the scanning electron micrographs of the xerogels was performed. The SEM showed the formation of compact fibrous structures, wherein each fiber was found to be actually made up of intertwining of thinner fibrils **(Figure 4.3.5.13).**

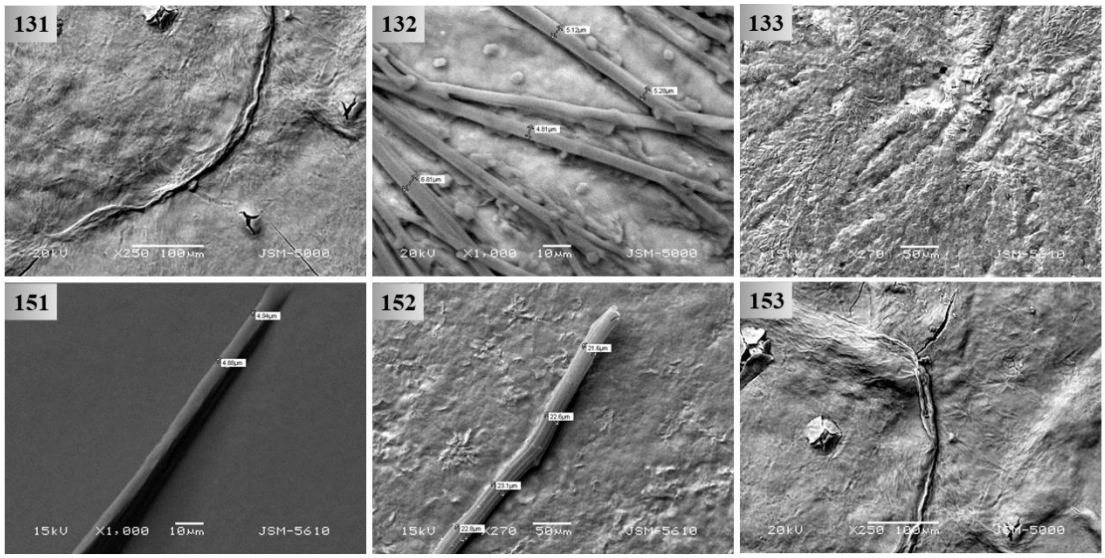

Figure 4.3.5.13 SEM images showing the fibrous network in the metallogels which are responsible for gel formation.

4.4 Metallogels as Catalysts for Oxidation

Copper is considered an important bio-essential element since long, however the importance of copper has been recognized in the past 30-40 years because of the development of bioinorganic chemistry. Copper containing enzymes are an integral part of the living systems. Type III copper proteins have coupled binuclear copper centers as their active sites. Type III copper active site is present in hemocyanin (O_2 transport), tyrosinase (hydroxylation of monophenols and oxidation of catechols), and several multicopper oxidases. The active site in ascorbic acid oxidase and laccase is known to be a trinuclear active centre with a combination of Type II and Type III sites.[41–43] The ability to oxidize *ortho*-diphenols is important in medical diagnosis for determination of hormonally active catecholamines, adrenaline, noradrenaline and dopa.[44,45] The direct use of these metalloproteins is difficult for their availability and stability in vitro while the synthetic mimics which function as highly efficient catalysts can be used to overcome this difficulty.[46,47] Many complexes having copper(II) have been designed and synthesized as enzyme mimics/models of metalloprotein/metalloenzymes containing copper.[48–52] Some of them have been shown to possess catecholase activity.[46,47,53–60] The studies on the model compounds mimicking the oxidase type activity are useful and promising for the development of new, more efficient bioinspired, environment friendly catalysts, for in vitro oxidation reactions.

The copper containing enzymes owe their activity to the presence of copper(II) as a redox active centre. A tricopper(II) species is the main component of the metallogels reported in this chapter. Hence, it was thought of interest to explore their ability to catalyse the oxidation of various phenols. 3,5-di-*tert*-butylcatechol (3,5-DTBC) has been used as a convenient model substrate in most of the reports of synthetic models of catecholase enzymes. However, the metallogelator complex being a tricopper(II) species, it was thought of interest to consider its ability to catalyse the oxidation of various types of diphenols instead of restricting to catechol and 3,5-di-*tert*-butylcatechol. The catalytic property of the gels has been tested using pyrocatechol, 3,5-di-*tert*-butylcatechol, 4-methyl catechol, 2,3-dihydroxy naphthalene, resorcinol and hydroquinone. This is the first report of catalytic oxidation of substrates like 2,3-dihydroxy naphthalene, hydroquinone and resorcinol with atmospheric oxygen as oxidant. Also, this is the first report of using metallogels as heterogeneous catalysts for aerobic oxidation of diphenols.

The metallogels at the end of the oxidation process were regenerated and they can be again used for oxidation in further catalytic cycles.

The ease of separation of the product after the reaction, faster oxidation processes and regeneration of metallogels make these gels excellent heterogeneous catalysts for such oxidation processes.

4.4.1 Oxidation of 4-methyl catechol using metallogels

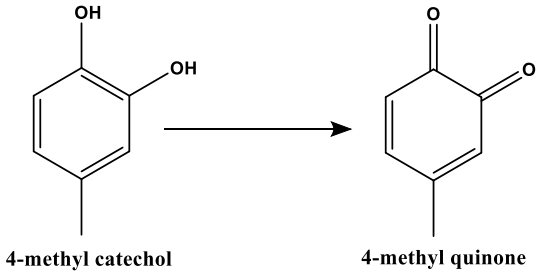

Scheme 4.4.1.1 Scheme showing the oxidation of **4-methyl catechol** to **4-methyl quinone.**

The **metallogels (131, 132, 133)** were used as catalyst in the oxidation of 4-methyl catechol to 4-methyl quinone. As the metallogel is soluble in methanol, a rigid and hard gel was prepared that resists the sol-gel transformation or solubilization even under the influence of a methanol layer placed above it during the oxidation activity. The **metallogel-132** was formed in a vial over which methanol solution was added in the ratio of 1:10 = metallogelator complex: 4-methyl catechol **(Figure 4.4.1.1)**.

As seen in the **Figure 4.4.1.1**, as soon as methanol solution containing 4-methyl catechol was poured on the surface of the metallogel, oxidation of the substrate starts instantaneously. This instantly results in the appearance of brownish colour solution which is an indication of the formation of the diquinone, the oxidized product of 4-methyl catechol. UV-visible spectroscopy was also used to monitor the oxidation of 4-methyl catechol to 4-methyl quinone an absorption peak corresponding to the quinone appeared at 412 nm. In order to monitor the formation of 4-methyl quinone, 1.25 mL of the **metallogel-132 (0.083 moles)** was prepared in a cuvette and a solution of 4-methyl catechol **(4.06 mM)** in 1 mL methanol and poured on the surface of the metallogel. The intensity of peak at **412 nm** increases with time **(Figure 4.4.1.2)**. Methanol was chosen as a solvent of choice, as both the substrate and the reaction product are soluble in methanol. This is the first ever report of oxidation of 4-methyl catechol using a metallogel as a heterogeneous catalytic system. As the metallogel contains copper(II), the oxidation happens at the surface of the metallogel. As the

product is soluble is methanol, the product can easily be recovered just by decanting the methanol solution leaving behind, the metallogel intact. Thus, by using a metallogelator system very effective recovery can be achieved after the oxidation process. The metallogelator surface after the oxidation activity was washed 4-5 times with methanol in order to clean the surface of the metallogel and it was once again used for the next catalytic cycle. The gel remains intact till 5 catalytic cycles.

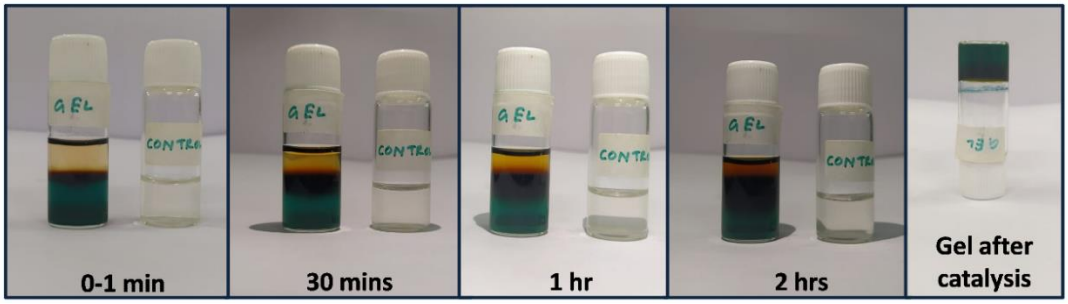

Figure 4.4.1.1 Visual change showing the oxidation of 4-methyl catechol to 4-methyl quinone using metallogel 132 as a heterogeneous catalyst.

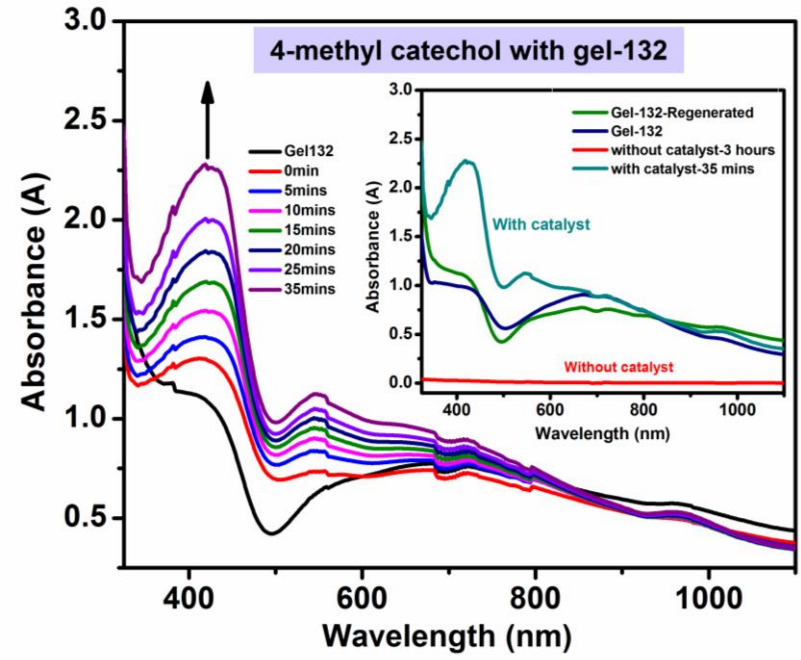

Figure 4.4.1.2 UV-Visible spectrum showing the oxidation of 4-methyl catechol to 4-methyl quinone using the **metallogel-132**. The figure in the inset shows the regeneration of the gel after the oxidation activity.

The product 4-methyl quinone shows a strong absorbance at λ_{max} = 412nm (ε= 1900 $dm^3\,mol^{-1}\,cm^{-1}$) and also it is stable. From the **Figure 4.4.1.1** it is evident that the intensity of the peak at ~ 412 nm increases along with time indicating progressive oxidation of 4-methyl catechol to 4-methyl quinone.

As shown in the **Figure 4.4.1.1(inset)** the UV-Vis spectrum of the metallogel before and after the oxidation with 4-methyl catechol remained same which proves that the metallogel was regenerated after the oxidation activity. To record the UV-Vis spectrum of the regenerated metallogel the surface of the gel was washed 4-5 times with methanol in order to make the surface of the metallogel free from the quinone layer. This leads to a slight decrease in the absorption intensity of the regenerated gel owing to the slight leaching of the metallogel from the surface during methanol washing. On comparison of the oxidation of 4-methyl catechol in presence and absence of catalyst it is observed that there is no oxidation of 4-methyl catechol in absence of the catalyst even after 3 hours.

Oxidation of 4-methyl catechol using metallogel-131

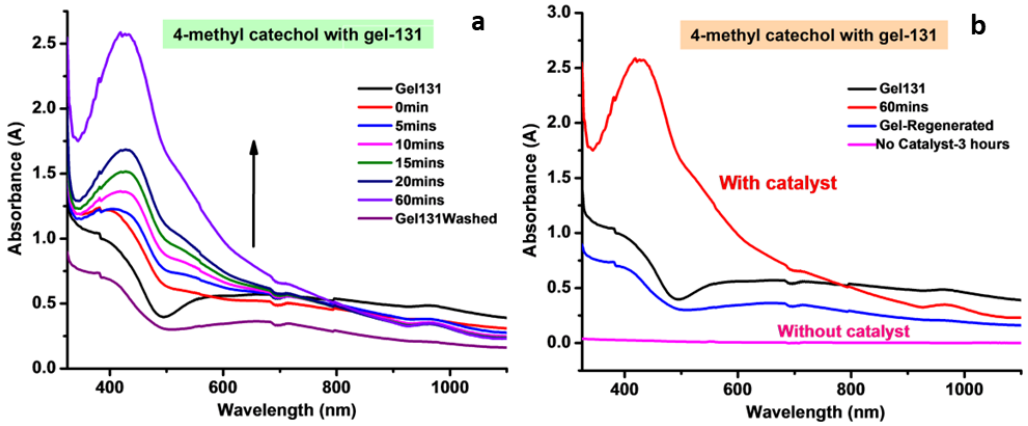

Figure 4.4.1.3 (a) UV-Visible spectrum showing the oxidation of 4-methyl catechol to 4-methyl quinone using the **metallogel-131**. **(b)** UV-visible spectrum showing the regeneration of the gel after the oxidation activity.

Oxidation of 4-methyl catechol using metallogel-133

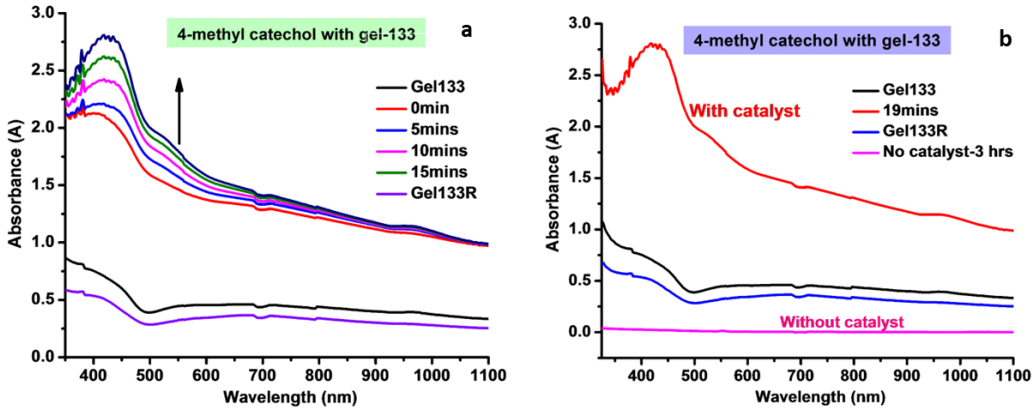

Figure 4.4.1.4 (a) UV-Visible spectrum showing the oxidation of 4-methyl catechol to 4-methyl quinone using the **metallogel-133**. **(b)** UV-visible spectrum showing the regeneration of the gel after the oxidation activity.

Regeneration of metallogel after oxidation activity

The regeneration of the metallogels after the oxidation of 4-methyl catechol to 4-methyl quinone is ascertained with the help of various spectroscopic and microscopic studies. In addition to the UV-Vis spectra, ESR and FT-IR spectra of the metallogels before and after the reaction were compared. Oxidation activity carried out using metallogel-132 was chosen as a representative case for these studies.

The SEM analysis of the gels was performed before and after the catalytic activity to check if there is any change in the morphology of the gel-forming assembly. It was observed that the fibrous assembly in the gels still remained intact as can be as seen from the **Figure 4.4.1.5.**

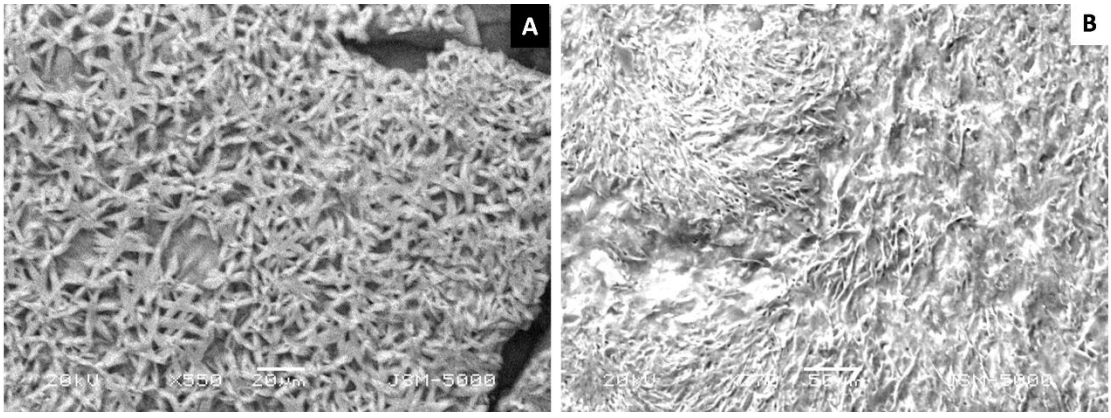

Figure 4.4.1.5 SEM images showing the presence of fibrous assembly of the **metallogel-132 (A)** before and after **(B)** the catecholase activity with 4-methyl catechol.

The d-d transition observed in the UV-Visible spectra **(Figure 4.4.1.2)** of the gel before and after the catalytic activity remains identical and the transitions correspond to those in a d^9 system, i.e. copper(II). The ESR spectra (**Figure 4.4.1.6)** also confirm the presence of copper ions in +2 oxidation state.

The ESR spectra of metallogel-132 before and after the catalysis recorded in aqueous solution form at room temperature is a typical axial ESR of S=1/2 system corresponding to copper(II) centre in axial environment. A well resolved hyperfine structure due to coupling of the electron spin with the nuclear spin of I=3/2 is observed. Four discernible lines in the $g_{\|}$ region are observed for metallogel-132 with an average $A_{\|}$ value = 68.07 x 10^{-4} cm^{-1} ($g_{\|}$ = 2.1412 and $g_{\perp}$ = 2.0454) and an average A|| value = 65.97 x 10^{-4} cm^{-1} ($g_{\|}$ = 2.1381 and $g_{\perp}$ = 2.0472) and for metallogel-132 after using it as a oxidation catalyst.

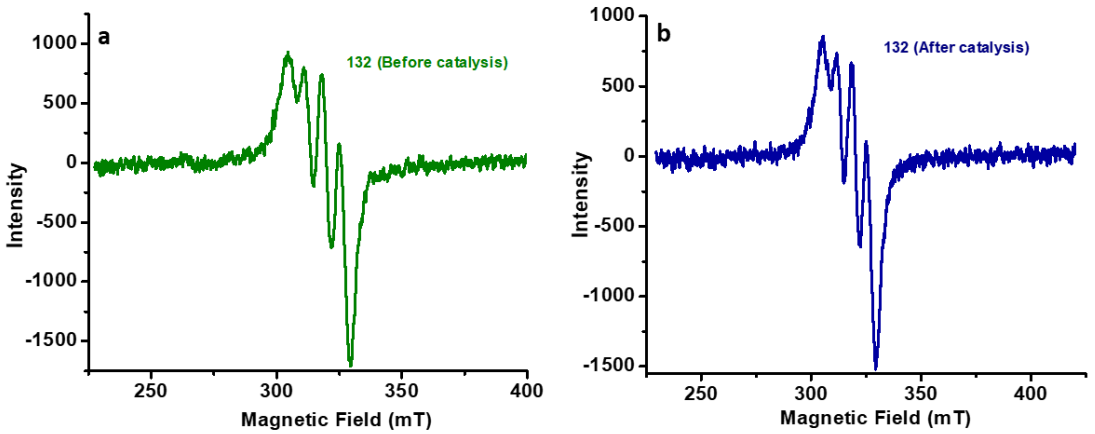

Figure 4.4.1.6 Figure (a) and (b) showing the ESR spectrum of metallogel 132 before and after the catalytic processes respectively.

Further, the ESR spectra of the gels recorded before and after the catalytic reactions are identical indicating that there is no change in the coordination environment of the copper ions.

FT-IR of metallogels used in the catalytic oxidation of 4-methyl catechol

FT-IR data for xerogel 132 (before oxidation activity): FT-IR, cm^{-1} (KBr): 3418.30, 2924.45,2853.74, 1602.50,1470.37, 1446.06, 1376.83, 1156.16, 1112.34, 1028.77, 950.62, 894.66, 778.79, 731.93, 546.61 **(Figure 4.4.1.7-a)**

FT-IR data for xerogel 132(after oxidation activity): FT-IR, cm^{-1} (KBr): 3419.04, 2924.21, 2353.40,1601.39, 1470.14, 1445.47, 1377.86, 1316.93, 1201.65, 1156.52, 1112.83, 1026.67, 950.28, 894.62, 778.38, 732.10, 545.14 **(Figure 4.4.1.7-b)**

FT-IR spectrum as seen from the **Figure 4.4.1.7** of the metallogelator complex post catalytic activity also shows that the chemical structure of the gel forming complex does not change after the oxidation activity.

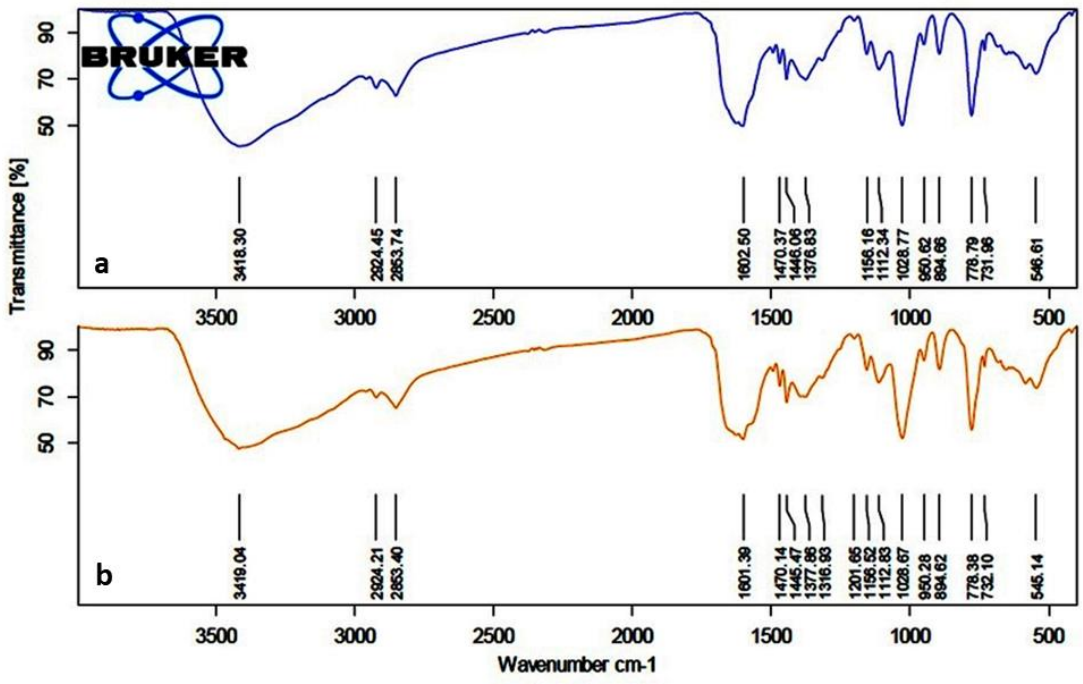

Figure 4.4.1.7 FT-IR spectra of the **xerogel 132 (a)** before and **(b)** after the oxidation activity with 4-methyl catechol.

4.4.2 Oxidation of 3,5-DTBC using metallogels

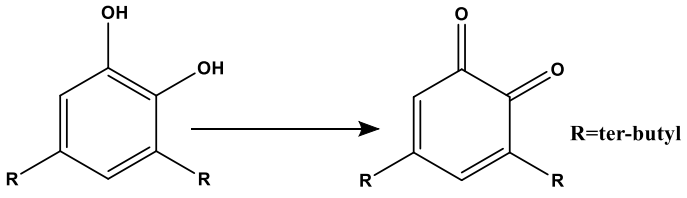

3,5-DTBC 3,5-DTBQ

Scheme 4.4.2.1 Scheme showing the oxidation of **3,5-DTBC** to **3,5-DTBQ.**

Similar experiments were performed to examine the catalytic activity of the metallogels for the oxidation of **3,5-DTBC (3,5-di-tert-butyl-o-catechol)** as a substrate. A layer of dichloromethane, CH_2Cl_2, containing the substrate 3,5-DTBC was added to the priorly prepared metallogel-132 in the metallogelator complex:3,5-DTBC ratio of 1:10. 1.25 mL of the **metallogel-132 (0.083 moles)** was formed in a cuvette and a solution of 3,5-DTBC **(4.06 mM)** dissolved in 1 mL dichloromethane was added on the surface of the metallogel. As soon as the substrate comes in contact with the metallogel, the oxidation of the substrate starts instantaneously, at the interface of the metallogel and the dichloromethane layer. The progress of the reaction is indicated by the appearance of yellowish-brown colour which intensifies with time **(Figure 4.4.2.1)**. In order to monitor the oxidation of the substrate, UV-Visible spectra have been recorded wherein

the absorbance at λ_{max} = 405nm corresponding to 3,5-DTBQ was monitored. The intensity of the peak at λ_{max} = 405 nm goes on increasing indicating the progress of oxidation of DTBC in presence of metallogel-132 as catalyst **(Figure 4.4.2.2)**.

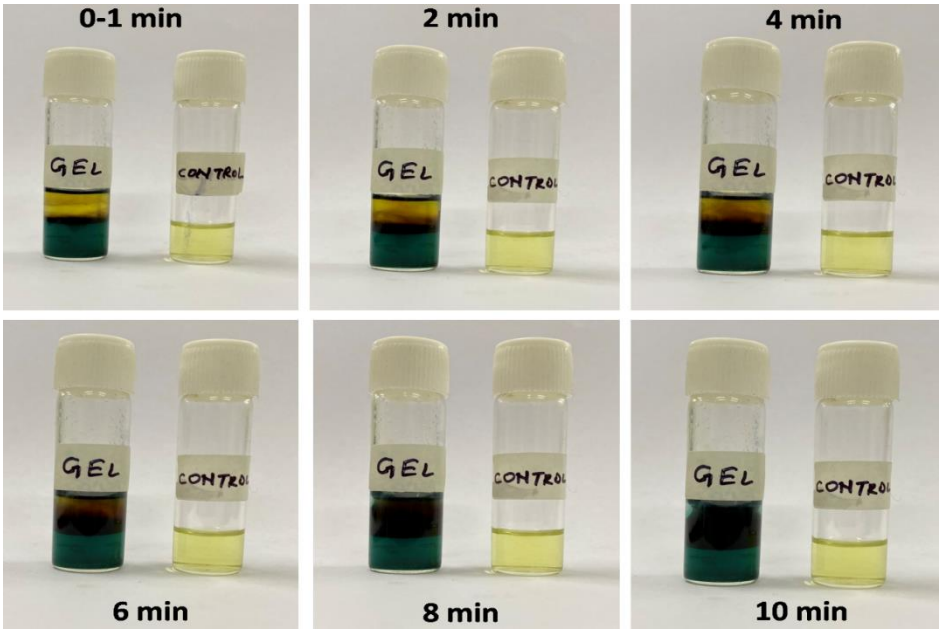

Figure 4.4.2.1 Oxidation of **3,5-DTBC** to **3,5-DTBQ** using metallogel 132 as a heterogeneous catalyst.

From the above figure the intensification of colour due to the formation of DTBQ is evident. In the UV-vis spectra (**Figure 4.4.2.2)**, the intensity of peak corresponding to DTBQ, at 405 nm increases with time indicating the progressive oxidation of 3,5-DTBC to 3,5-DTBQ. An additional peak having an absorption maximum at 576 nm appears during the reaction indicating the formation of an unstable intermediate between the copper(II) centres of the metallogel and 3,5-DTBC. It was found that the intensity of this peak initially increases **(till 19 minutes in case of metallogel 132)** followed by a decrease in the intensity of the peak towards the completion of the reaction.

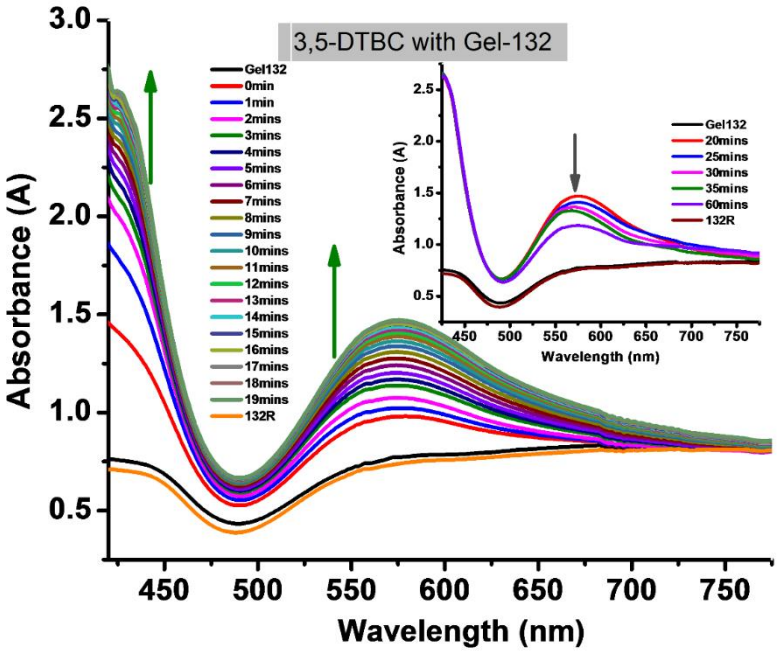

Figure 4.4.2.2 UV-Visible spectra exhibiting the monitoring of 3,5-di-tert-butyl-o-quinone (3,5-DTBQ) from 3,5-DTBC in presence of metallogel-132. Inset figure shows the decay of the intermediate after 20 min.

After the entire 3,5-DTBC was oxidized to 3,5-DTBQ the dichloromethane layer was decanted and the metallogel was washed with cold methanol. The UV-Vis spectrum of the metallogel before and after the oxidation activity was found to be same indicating the regeneration of metallogel after the catalytic process.

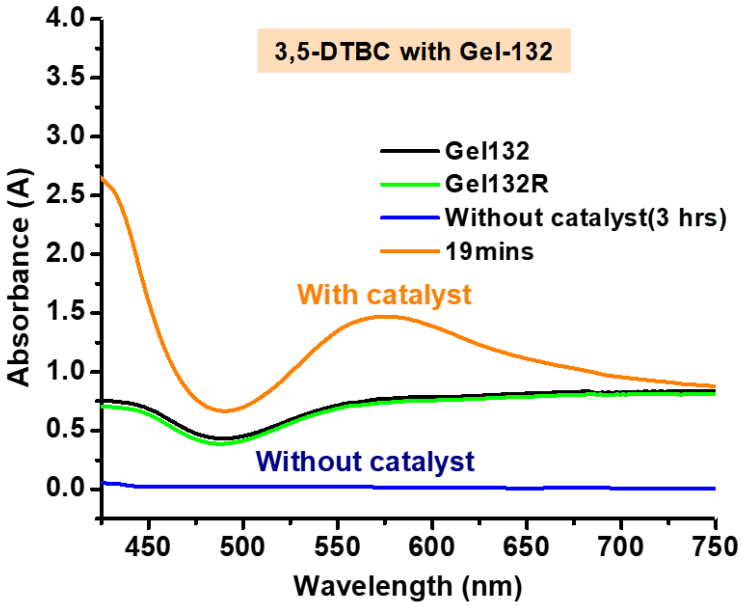

Figure 4.4.2.3 UV-Visible spectra of (i) DTBC alone initially and after 3 hrs.(blue), (ii) DTBC with catalyst during the reaction (orange), (iii) Gel 132 (purple), (iv) Gel 132 regenerated after the oxidation of the substrate(green).

As seen from the UV-Visible spectra represented in **Figure 4.4.2.3** it can be seen that the arial oxidation of 3,5-DTBC which was recorded after 3 hours is negligible in absence of the metallogel which catalyses the oxidation process.

Similar catalytic activity with 3,5-DTBC as a substrate and consequent recovery of the metallogels after the activity was done using metallogels **131** and **133** (**Figure 4.4.2.4 and Figure 4.4.2.5**)

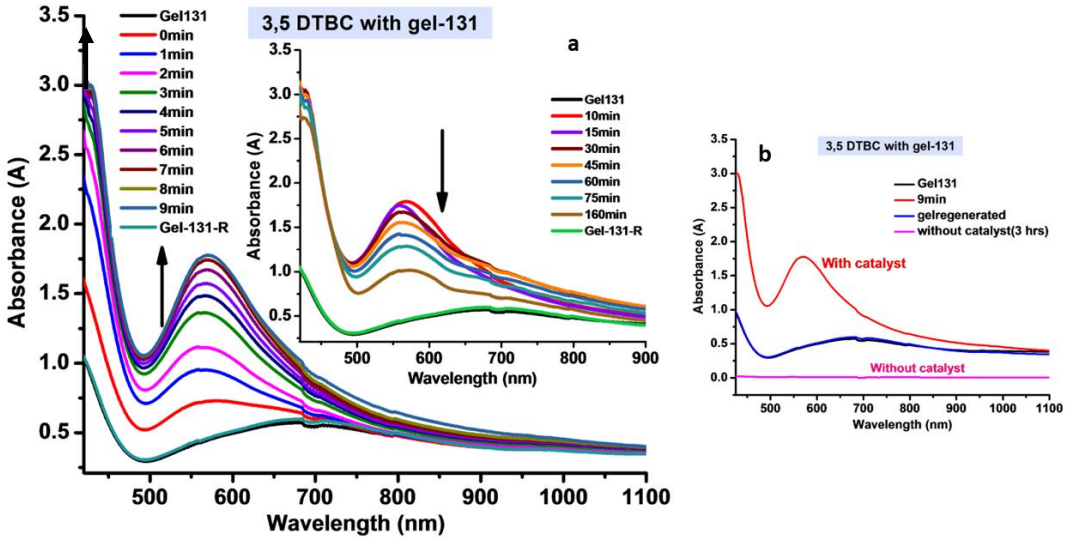

Figure 4.4.2. UV-Visible spectrum of DTBC in presence of the **metallogel-131.** Inset figure (a) showing the decay of the intermediate formed during the reaction after 10 min. (b) The substrate alone (pink), substrate with catalyst during the reaction (red) and the metallogel catalyst before and after the reaction (purple and blue).

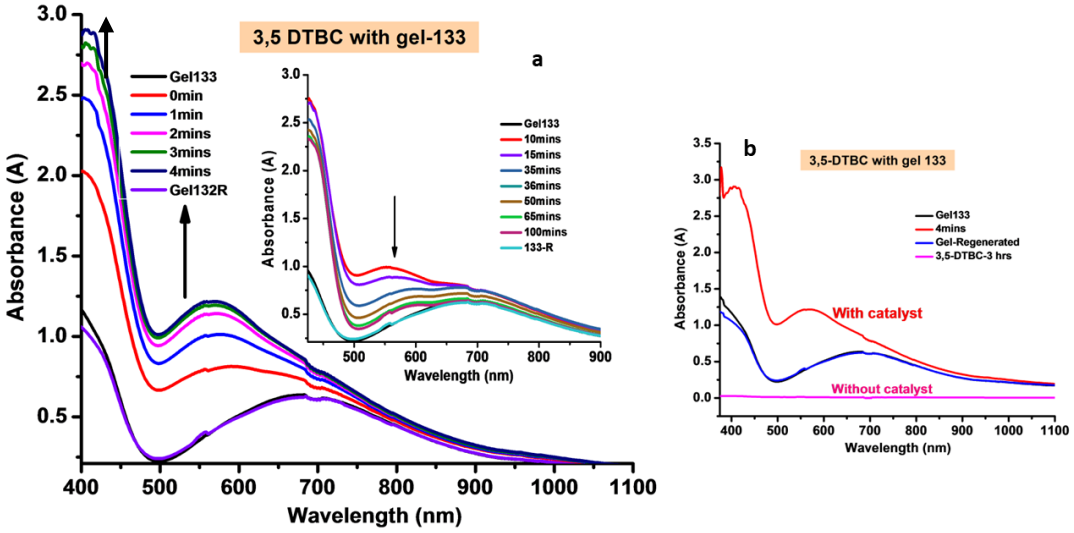

Figure 4.4.2.6 UV-Visible spectrum of DTBC in presence of the **metallogel-133.** Inset figure (a) showing the decay of the intermediate formed during the reaction after 10 min. (b) The substrate alone (pink), substrate with catalyst during the reaction (red) and the metallogel catalyst before and after the reaction (purple and blue).

Since all metallogels reported here were found to be catalysts for the oxidation of DTBC and 4-methyl catechol, the **metallogel 132** was selected as a representative for further experiments with other diphenols. The catalytic oxidation of 2,3-dihydroxy naphthalene, resorcinol, hydroquinone and pyrocatechol with arial oxygen in presence of **metallogel 132** has been examined. The oxidation in each of the cases was monitored using UV-Visible spectroscopy. The metallogel was regenerated at the end of the catalytic process as in the cases discussed before. These are the first ever reports of this kind for the substrates other than catechol derivatives. There have been no reports on the catalytic oxidation of 2,3-dihydroxy naphthalene, resorcinol and hydroquinone by using either homogenous or heterogeneous catalysts let alone metallogels.

4.4.3 Oxidation of 2,3-Dihyroxynaphthalene using metallogel-132

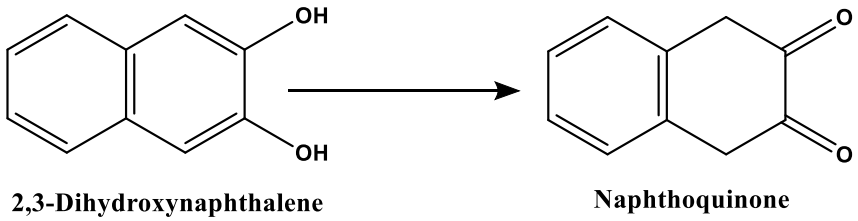

2,3-Dihydroxynaphthalene **Naphthoquinone**

Scheme 4.4.3.1 Scheme showing the oxidation of **2,3-Dihydroxynaphthalene** to **Naphthoquinone.**

A layer of dichlorimethane containing the substrate **2,3-Dihyroxynaphthalene** was added to the previously prepared metallogel-132 in a glass vial **(Figure 4.4.3.1)** in the ratio of 1:10 = metallogelator complex: substrate.

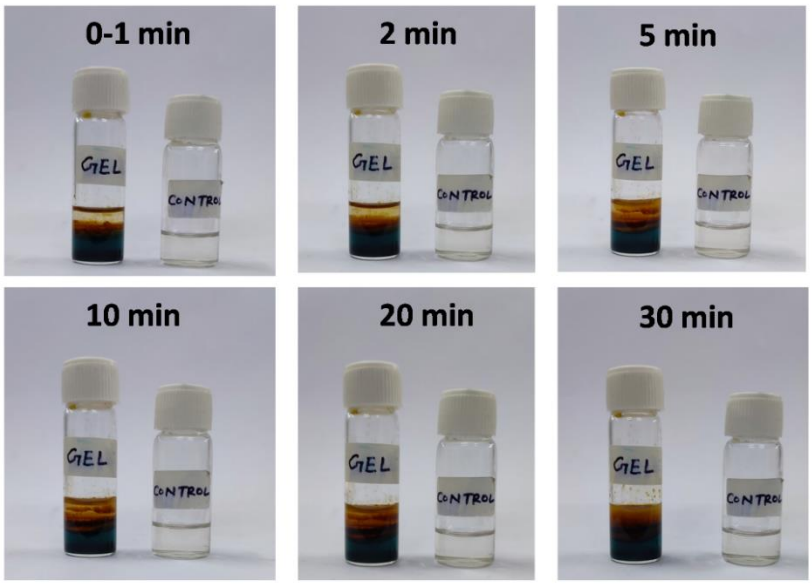

Figure 4.4.3.1 Oxidation of **2,3-Dihydroxynaphthalene** to **Naphthoquinone** over the surface of the metallogel-132.

As soon as the substrate comes in contact with the metallogel, the oxidation of the substrate starts at the interface of the metallogel and dichloromethane layer. The progress of the reaction is indicated by the appearance of yellowish-brown colour which intensifies with time **(Figure 4.4.3.1)**.

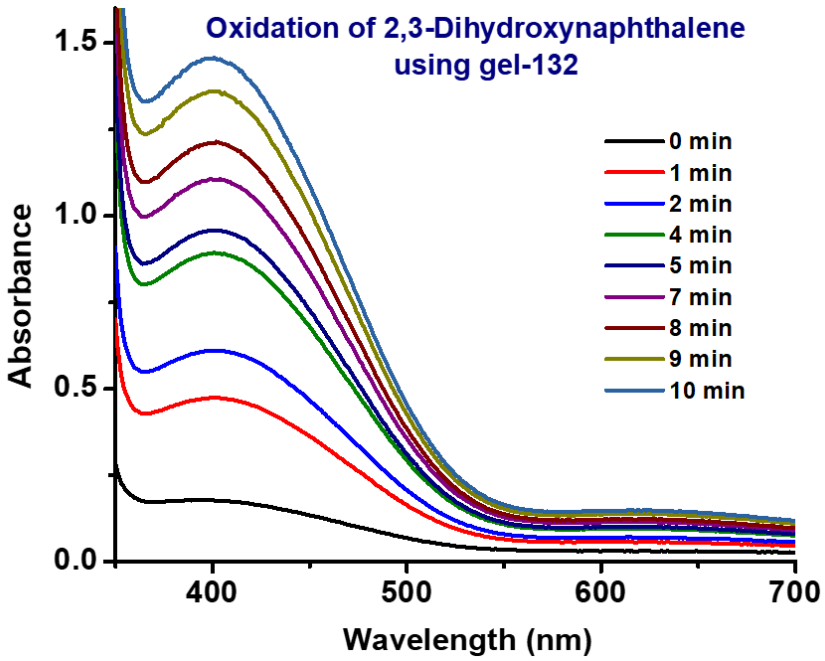

Figure 4.4.3.2 UV-Visible studies showing the oxidation of **2,3-Dihydroxynaphthalene** to **Naphthoquinone** using the **metallogel-132.**

In order to quantitatively monitor the formation of the substrate during the oxidation reaction, UV-Visible spectra have been recorded wherein the absorbance at λ_{max} **= 395 nm** corresponding to formation of **naphthoquinone** was monitored. **1.25 mL** of the **metallogel-132 (0.083 moles)** was formed in a cuvette and a solution of **2,3-dihydroxynaphthalene (2.03 mM)** dissolved in 1mL dichloromethane (MDC) + 1 mL methanol was added on the surface of the metallogel. As seen from the **Figure 4.4.3.2** the intensity of the peak of **naphthoquinone** at λ_{max} **= 395 nm** goes on increasing indicating the progress of oxidation of the substrate using metallogel-132 as catalyst**.**

4.4.4 Oxidation of pyrocatechol (1,2-Dihydroxybenzene) using metallogel-132

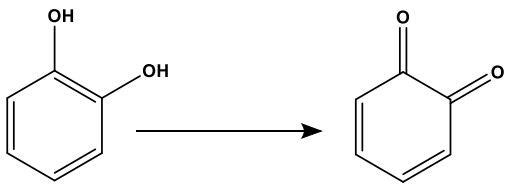

Scheme 4.4.4.1 Scheme showing the oxidation of **pyrocatechol** to **1,2-Benzoquinone.**

In order to carry out the oxidation of **pyrocatechol** a layer of methanol containing the substrate **pyrocatechol** was added to the priorly prepared metallogel-132 in a glass vial **(Figure 4.4.4.1)** in the ratio of 1:10 = metallogelator complex: pyrocatechol.

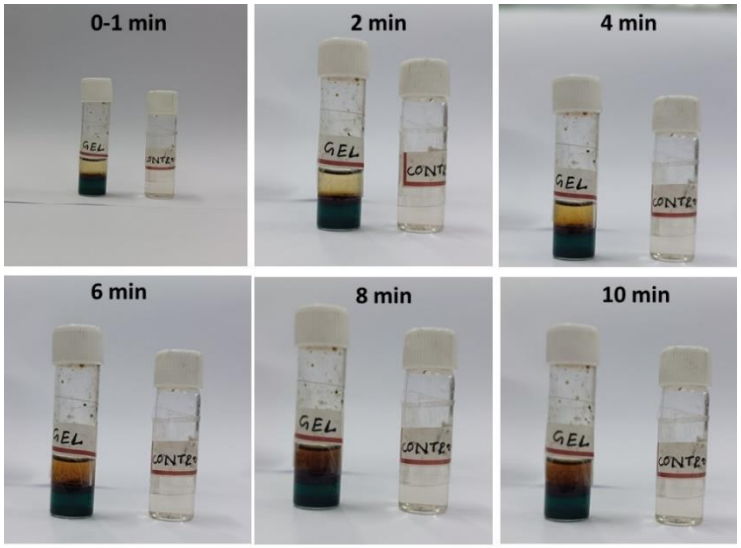

Figure 4.4.4.1 Oxidation of **pyrocatechol** to **1,2-benzoquinone** over the surface of the metallogel-132 formed in the vial.

As soon as the substrate comes in contact with the metallogel, the oxidation of the substrate starts at the interface of the metallogel and methanol. The progress of the reaction is indicated by the appearance of yellowish-brown colour which intensifies with time **(Figure 4.4.4.1)**.

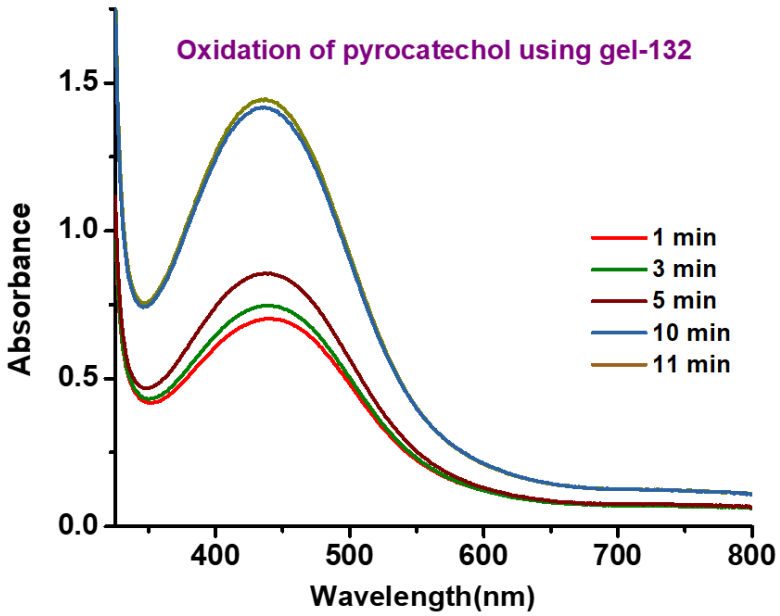

Figure 4.4.4.2 UV-Visible studies showing the oxidation of **pyrocatechol** to **1,2-benzoquinone** using the **metallogel-132.**

In order to quantitatively monitor the formation of the substrate during the oxidation reaction, UV-Visible spectra were recorded wherein the absorbance at λ_{max} **= 435 nm** corresponding to formation of **1,2-Benzoquinone** was monitored. **1.25 mL** of the **metallogel-132 (0.083 moles)** was formed in a cuvette and a solution of **pyrocatechol (2.03 mM)** was dissolved in 1mL dichloromethane (MDC) + 1 mL methanol and poured on the surface of the metallogel. As seen from the **Figure 4.4.4.2** the intensity of the peak at λ_{max} = **435 nm** goes on increasing indicating the progress of oxidation of the substrate using metallogel-132 as catalyst**.**

4.4.5 Oxidation of Resorcinol (1,3-dihyroxybenzene) using metallogel-132

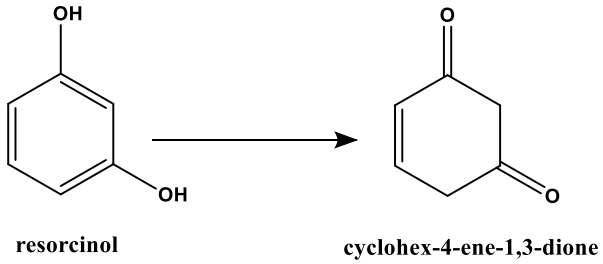

Scheme 4.4.5.1 Scheme showing the oxidation of **resorcinol** to **cyclohex-4-ene-1,3-dione**

In order to carry out the oxidation of **resorcinol**, a layer of dichloromethane containing the substrate was added to the previously prepared metallogel-132 in a glass vial **(Figure 4.4.5.1)** in the ratio of 1:10 = metallogelator complex: substrate.

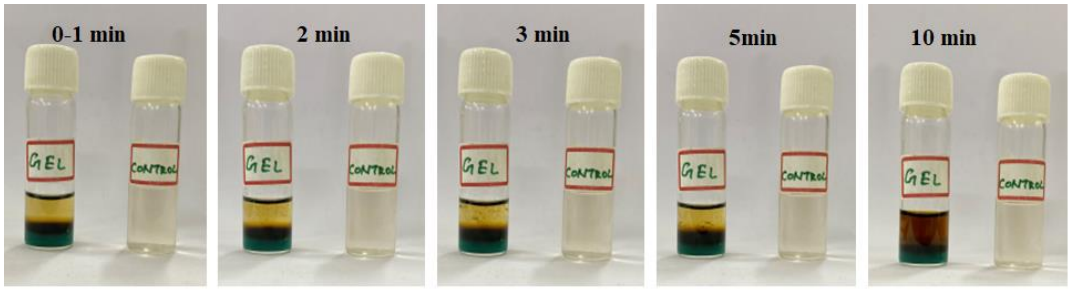

Figure 4.4.5.1 Oxidation of **Resorcinol** over the surface of the **metallogel-132** formed in the vial.

The oxidation of the substrate starts immediately at the interface of the metallogel and dichloromethane as it is added onto the surface of the gel. The progress of the reaction is indicated by the appearance of yellowish-brown colour which intensifies with time **(Figure 4.4.5.1)**.

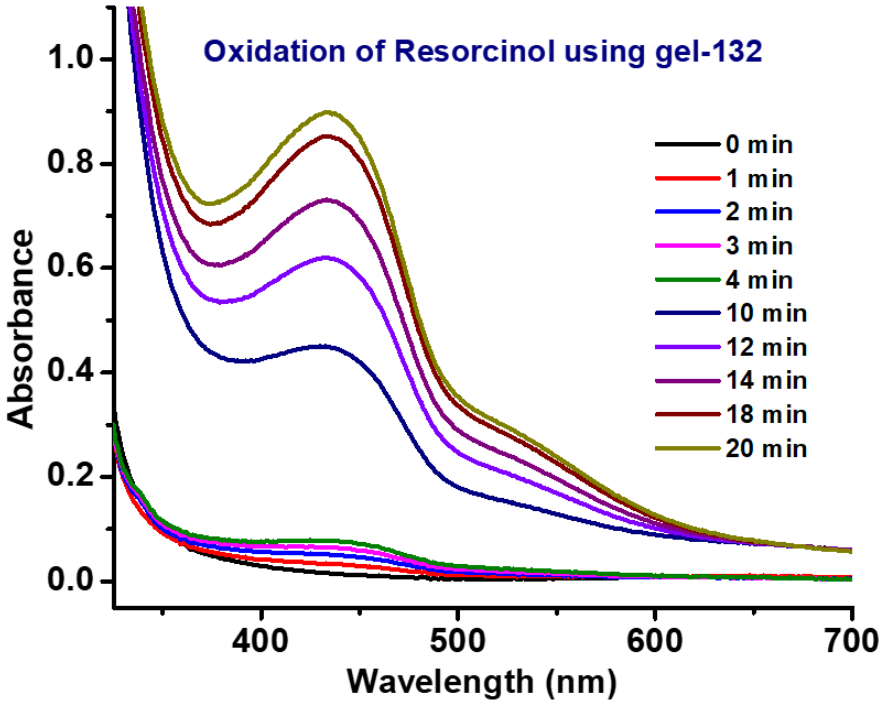

Figure 4.4.5.2 UV-Visible studies showing the oxidation of **resorcinol** using the **metallogel-132.**

UV-Visible spectroscopy was used to monitor the formation of the substrate during the oxidation reaction. **1.25 mL** of the **metallogel-132 (0.083 moles)** was formed in a cuvette and a solution of **resorcinol (2.03 mM)** dissolved in 1mL dichloromethane (MDC) + 1 mL methanol was added on the surface of the metallogel prepared inside the cuvette. The absorbance at λ_{max} **= 435 nm** corresponding to formation of **cyclohex-4-ene-1,3-dione** was monitored. As can be seen in the **Figure 4.4.5.2,** the intensity of the peak at λ_{max} **= 435 nm** goes on increasing with time indicating the progress of oxidation of the substrate in presence of metallogel-132 as a catalyst**.**

4.4.6 Oxidation of hydroquinone (1,4-dihyroxybenzene) using metallogel-132

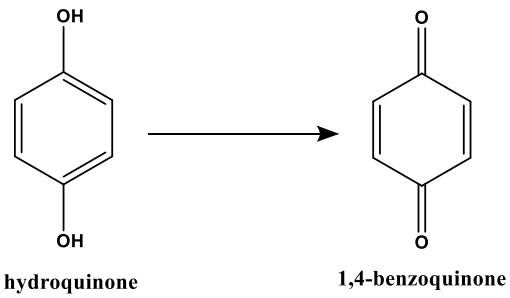

Scheme 4.4.6.1 Scheme showing the oxidation of **hydroquinone** to **1,4-benzoquinone.**

Oxidation of **hydroquinone** was carried out by adding a layer of dichloromethane containing the substrate onto the previously prepared metallogel-132 in a glass vial **(Figure 4.4.6.1)** in the ratio of 1:10 = metallogelator complex: hydroquinone.

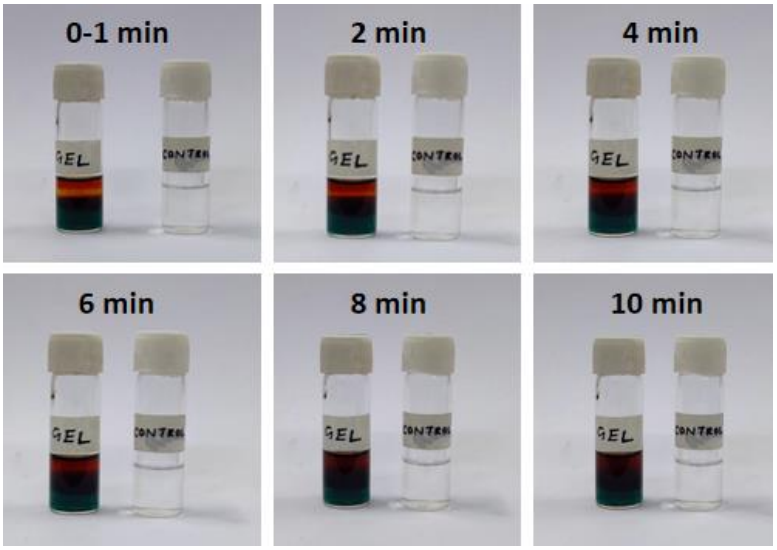

Figure 4.4.6.1 Oxidation of **hydroquinone to 1,4-benzoquinone** over the surface of the **metallogel-132** formed in the vial.

As soon as the substrate comes in contact with the metallogel, the oxidation of the substrate starts at the interface of the metallogel and dichloromethane layer. The reaction can be visibly seen as there is appearance of yellowish-brown colour which intensifies with time **(Figure 4.4.6.1)**.

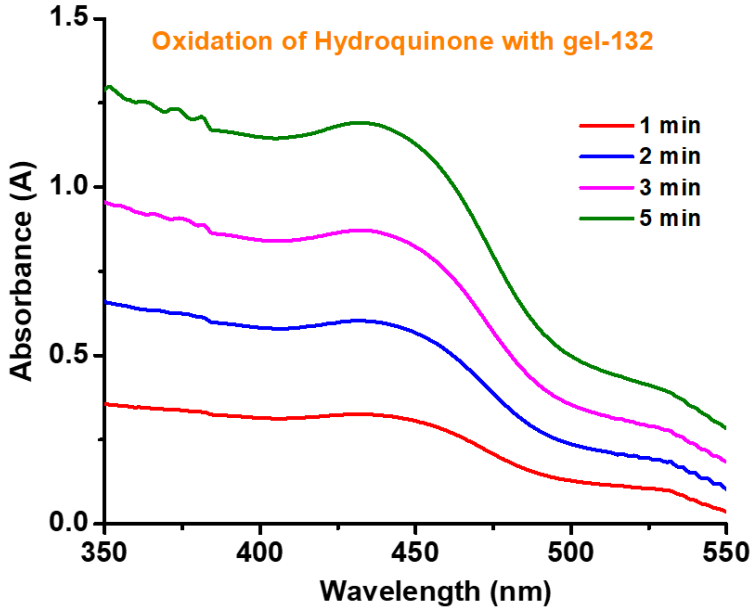

Figure 4.4.6.2 UV-Visible studies showing the oxidation of **hydroquinone to 1,4-benzoquinone** using the **metallogel-132.**

In order to quantitatively monitor the formation of the substrate during the oxidation reaction, UV-Visible spectra were recorded wherein the absorbance at λ_{max} **= 435 nm** corresponding to formation of **1,2-benzoquinone** was monitored. **1.25 mL** of the **metallogel-132 (0.083 moles)** was formed in a cuvette and a solution of **hydroquinone (2.03 mM)** dissolved in 2mL of dichloromethane + methanol (1:1) was added on the surface of the metallogel formed inside the cuvette. As seen from the **Figure 4.4.6.2** the intensity of the peak at λ_{max} **= 435 nm** goes on increasing indicating the progress of oxidation of the substrate using metallogel-132 as catalyst**.**

Thus, the metallogels behave as good catalysts for the oxidation of 1,2-, 1,3- and 1,4-diphenols to the corresponding quinone using atmospheric oxygen as oxidant under ambient conditions.

4.5 Conclusions

- 6 Novel Metallogels formed because of the trinuclear copper(II) system bound to 2,2'-bipyridine and myo-inositol as ligands were synthesised. The metallogels reported in this chapter were synthesized at pH of 8.5-9 which is very close to the physiological pH values, in contrary to the gels reported in chapter 2. This could be achieved using carbonate bases like K_2CO_3 and Na_2CO_3.

- T_{gel} values have been found to be highly dependent on the type of the carbonate base and counter anions used in the synthesis of the metallogels.

- The metallogels have been characterized by UV-vis spectroscopy and the structure of the trinuclear complex was proved by ESI-MS and FT-IR analysis. The SEM and POM images show the presence of fibrous assemblies and birefringence, respectively.

- The gels were further used as catalysts to carry out oxidation of various substrates like 3,5-di tert-butylcatechol (3,5-DTBC), 4-methyl catechol, 2,3-dihydroxy naphthalene, hydroquinone, resorcinol and pyrocatechol, the oxidation product of which was monitored using UV-Vis spectroscopy. The metallogels at the end of the oxidation process were regenerated and can be reused for oxidation in further catalytic cycles. The ease of separation of the product post reaction, faster oxidation processes and regeneration of metallogels make these gels excellent heterogeneous catalysts for such oxidation processes.

- It is for the first time metallogels have been used as heterogenous catalysts, in which the oxidation reactions of substrates take place at the interface.

- These are the first reports of its kind exhibiting the catalytic oxidation of substrates like 2,3-dihydroxy naphthalene, hydroquinone and resorcinol by molecular oxygen under ambient conditions.

References

1. Terech, P. & Weiss, R. G. Low Molecular Mass Gelators of Organic Liquids and the Properties of Their Gels. *Chem. Rev.* **2665**, 3133−3159 (1997).

2. *Molecular Gels: Materials With Self- Assembled Fibrillar Networks, (Eds. R. G. Weiss and P. Terech)*. (Springer, Dordrecht, 2006).

3. Dastidar, P. Supramolecular gelling agents : can they be designed ? *Chem. Soc. Rev.* **37**, 2699–2715 (2008).

4. Esch, J. H. Van & Feringa, B. L. New Functional Materials Based on Self-Assembling Organogels : From Serendipity towards Design. *Angew. Chem. Int. Ed.* **39**, 2263–2266 (2000).

5. Xing, B., Choi, M. F. & Xu, B. A stable metal coordination polymer gel based on a calix[4]arene and its “uptake” of non-ionic organic molecules from the aqueous phase. *Chem. Commun.* 362–363 (2002).

6. Estroff, L. A. & Hamilton, A. D. Water Gelation by Small Organic Molecules Lara. *Chem. Rev.* **104**, 1201–1218 (2004).

7. Babu, S. S., Praveen, V. K. & Ajayaghosh, A. Functional π-gelators and their applications. *Chem. Rev.* **114**, 1973–2129 (2014).

8. Fenniri, H., Mathivanan, P., Vidale, K. L., Sherman, D. M., Hallenga, K., Wood, K. V. & Stowell, J. G. Helical rosette nanotubes: Design, self-assembly, and characterization. *J. Am. Chem. Soc.* **123**, 3854–3855 (2001).

9. Israelachvili, J. N. *Intermolecular and Surface Forces*. (Academic Press, New York, 3rd edn, 1991).

10. Ajayaghosh, A. & George, S. J. First phenylenevinylene based organogels: Self-assembled nanostructures via cooperative hydrogen bonding and π-stacking. *J. Am. Chem. Soc.* **123**, 5148–5149 (2001).

11. Wada, A., Tamaru, S., Ikeda, M. & Hamachi, I. MCM - Enzyme - Supramolecular Hydrogel Hybrid as a Fluorescence Sensing Material for Polyanions of Biological. *J. Am. Chem. Soc.* **131**, 5321–5330 (2009).

12. Yang, H., Liu, H., Kang, H. & Tan, W. Engineering Target-Responsive Hydrogels Based on Aptamer - Target. *J. Am. Chem. Soc.* **130**, 6320–6321 (2008).

13. Yoshimura, I., Miyahara, Y., Kasagi, N., Yamane, H., Ojida, A. & Hamachi, I. Molecular recognition in a supramolecular hydrogel to afford a semi-wet sensor chip. *J. Am. Chem. Soc.* **126**, 12204–12205 (2004).

14. Tiller, J. C. Increasing the local concentration of drugs by hydrogel formation. *Angew. Chemie - Int. Ed.* **42**, 3072–3075 (2003).

15. Friggeri, A., Feringa, B. L. & Van Esch, J. Entrapment and release of quinoline derivatives using a hydrogel of a low molecular weight gelator. *J. Control. Release* **97**, 241–248 (2004).

16. Lee, K. Y. & Mooney, D. J. Hydrogels for Tissue Engineering. *Chem. Rev.* **101**, 1869–1879 (2001).

17. Randall, J. P., Meador, M. A. B. & Jana, S. C. Tailoring Mechanical Properties of Aerogels for Aerospace Applications. *ACS Appl. Mater. Interfaces* **3**, 613–626 (2011).

18. Vemula, P. K. & John, G. Smart amphiphiles: Hydro/organogelators for in situ reduction of gold. *Chem. Commun.* **21**, 2218–2220 (2006).

19. Hatten, X. De, Bell, N., Yufa, N., Christmann, G. & Nitschke, J. R. A Dynamic Covalent , Luminescent Metallopolymer that Undergoes Sol-to-Gel Transition on Temperature Rise. *J. Am. Chem. Soc.* **133**, 3158–3164 (2011).

20. Rizzo, C., Marullo, S., Billeci, F. & D'Anna, F. Catalysis in Supramolecular Systems: the Case of Gel Phases. *European J. Org. Chem.* **22**, 3148–3169 (2021).

21. Xing, B., Choi, M. F. & Xu, B. Design of coordination polymer gels as stable catalytic systems. *Chem. - A Eur. J.* **8**, 5028–5032 (2002).

22. Tu, T., Assenmacher, W., Peterlik, H., Weisbarth, R., Nieger, M. & Dötz, K. H. An air-stable organometallic low-molecular-mass gelator: Synthesis, aggregation, and catalytic application of a palladium pincer complex. *Angew. Chemie - Int. Ed.* **46**, 6368–6371 (2007).

23. Tsuchiya, K., Orihara, Y., Kondo, Y., Yoshino, N., Ohkubo, T., Sakai, H. & Abe, M. Control of Viscoelasticity Using Redox Reaction. *J. Am. Chem. Soc.* **126**, 12282–12283 (2004).

24. Kawano, S., Fujita, N. & Shinkai, S. A Coordination Gelator That Shows a Reversible Chromatic Change and Sol - Gel Phase-Transition Behavior upon Oxidative / Reductive Stimuli. *J. Am. Chem. Soc.* **126**, 8592–8593 (2004).

25. Kishimura, A., Yamashita, T. & Aida, T. Phosphorescent Organogels via " Metallophilic " Interactions for Reversible RGB - Color Switching. *J. Agric. Food Chem* **127**, 179–183 (2005).

26. Weng, W., Beck, J. B., Jamieson, A. M. & Rowan, S. J. Understanding the Mechanism of Gelation and Stimuli-Responsive Nature of a Class of Metallo-Supramolecular Gels. *J. Am. Chem. Soc.* **128**, 11663–11672 (2006).

27. Tam, A. Y., Wong, K. M. & Yam, V. W. Unusual Luminescence Enhancement of Metallogels of Alkynylplatinum (II) 2 , 6-Bis (N -alkylbenzimidazol-2 ′ -yl) pyridine Complexes upon a Gel-to-Sol Phase Transition at Elevated Temperatures. *J. Am. Chem. Soc.* **131**, 6253–6260 (2009).

28. Kim, H. J., Lee, J. H. & Lee, M. Stimuli-responsive gels from reversible coordination polymers. *Angew. Chemie - Int. Ed.* **44**, 5810–5814 (2005).

29. Roubeau, O., Colin, A., Schmitt, V. & Clérac, R. Thermoreversible gels as magneto-optical switches. *Angew. Chemie - Int. Ed.* **43**, 3283–3286 (2004).

30. Rodríguez-Llansola, F., Miravet, J. F. & Escuder, B. A supramolecular hydrogel as a reusable heterogeneous catalyst for the direct aldol reaction. *Chem. Commun.* **47**, 7303–7305 (2009).

31. Singh, N., Conte, M. P., Ulijn, R. V., Miravet, J. F. & Escuder, B. Insight into the esterase like activity demonstrated by an imidazole appended self-assembling hydrogelator. *Chem. Commun.* **51**, 13213–13216 (2015).

32. Araújo, M., Díaz-Oltra, S. & Escuder, B. Triazolyl-Based Molecular Gels as Ligands for Autocatalytic 'Click' Reactions. *Chem. - A Eur. J.* **22**, 8676–8684 (2016).

33. Araújo, M., Capdevila, I. M., Díaz-Oltra, S. & Escuder, B. Tandem catalysis of an aldol-'click' reaction system within a molecular hydrogel. *Molecules* **21**, 744 (2016).

34. Araújo, M. & Escuder, B. Transient Catalytic Activity of a Triazole-based Gelator Regulated by Molecular Gel Assembly/Disassembly. *ChemistrySelect* **2**, 854–862 (2017).

35. Wang, G., Wang, D., Bietsch, J., Chen, A. & Sharma, P. Synthesis of Dendritic Glycoclusters and Their Applications for Supramolecular Gelation and Catalysis. *J. Org. Chem.* **85**, 16136–16156 (2020).

36. Jin, Q., Zhang, L., Cao, H., Wang, T., Zhu, X., Jiang, J. & Liu, M. Self-assembly of copper(II) ion-mediated nanotube and its supramolecular chiral catalytic behavior. *Langmuir* **27**, 13847–13853 (2011).

37. Hiscock, J. R., Bustone, G. P. & Clark, E. R. Decontamination and Remediation of the Sulfur Mustard Simulant CEES with "Off-the-Shelf" Reagents in Solution and Gel States:A Proof-of-Concept Study. *ChemistryOpen* **6**, 497–500 (2017).

38. Porcar, R., Burguete, M. I., Lozano, P., Garcia-Verdugo, E., Luis, S. V., Sarkar, S. S., Maji, P. K., Negishi, Y., Dutta, S., Das, T. N., Pan, R., Sarkar, S. S., Rizzo, C., Marullo, S., Billeci, F., D'Anna, F., Singh, N., Conte, M. P., *et al.* Cu(II)-Based Nanofibrous Metallogel for Phenoxazinone Synthase-like Activity. *ACS Sustain. Chem. Eng.* **4**, 1455–1466 (2021).

39. Malviya, N., Sonkar, C., Kundu, B. K. & Mukhopadhyay, S. Discotic Organic Gelators in Ion Sensing, Metallogel Formation, and Bioinspired Catalysis. *Langmuir* **34**, 11575–11585 (2018).

40. *Handbook of Liquid Crystals*. (Wiley-VCH, Weinheim, 1998).

41. Shin, W., Sundaram, U. M., Cole, J. L., Zhang, H. H., Hedman, B., Hodgson, K. O. & Solomon, E. I. Chemical and spectroscopic definition of the peroxide-level intermediate in the multicopper oxidases: Relevance to the catalytic mechanism of dioxygen reduction to water. *J. Am. Chem. Soc.* **118**, 3202–3215 (1996).

42. Machonkin, T. E., Quintanar, L., Palmer, A. E., Hassett, R., Severance, S., Kosman, D. J. & Solomon, E. I. Spectroscopy and reactivity of the type 1 copper site in Fet3p from Saccharomyces cerevisiae: Correlation of structure with reactivity in the multicopper oxidases. *J. Am. Chem. Soc.* **123**, 5507–5517 (2001).

43. Jones, S. M. & Solomon, E. I. Electron transfer and reaction mechanism of laccases. *Cell. Mol. Life Sci.* **72**, 869–883 (2015).

44. Rompel, A., Fischer, H., Meiwes, D., Büldt-Karentzopoulos, K., Dillinger, R., Tuczek, F., Witzel, H. & Krebs, B. Purification and spectroscopic studies on catechol oxidases from Lycopus europaeus and Populus nigra: Evidence for a dinuclear copper center of type 3 and spectroscopic similarities to tyrosinase and hemocyanin. *J. Biol. Inorg. Chem.* **4**, 56–63 (1999).

45. Than, R., Feldmann, A. A. & Krebs, B. Structural and functional studies on model compounds of purple acid phosphatases and catechol oxidases. *Coord. Chem. Rev.* **182**, 211–241 (1999).

46. Alves, W. A., Bagatin, I. A. & Da Costa Ferreira, A. M. Equilibria and tyrosinase activity of a dinuclear and its analogous tetranuclear imidazolate-bridged copper(II) complexes. *Inorganica Chim. Acta* **321**, 11–21 (2001).

47. González-Álvarez, M., Alzuet, G., Borrás, J., García-Granda, S. & Montejo-Bernardo, J. M. Structural and functional models for the dinuclear copper active site in catechol oxidases: Synthesis, X-ray crystal structures, magnetic and spectroscopic properties of μ-methoxo-bridged dinuclear copper(II) complexes with N-substituted sulfonamide ligan. *J. Inorg. Biochem.* **96**, 443–451 (2003).

48. Neves, A., Rossi, L. M., Bortoluzzi, A. J., Szpoganicz, B., Wiezbicki, C., Schwingel, E., Haase, W. & Ostrovsky, S. Catecholase activity of a series of dicopper(II) complexes with variable Cu-OH(phenol) moieties. *Inorg. Chem.* **41**, 1788–1794 (2002).

49. Tyeklár, Z. & Karlin, K. D. Copper–Dioxygen Chemistry: A Bioinorganic Challenge. *Acc. Chem. Res.* **22**, 241–248 (1989).

50. Kitajima, N. & Moro-oka, Y. Copper-Dioxygen Complexes. Inorganic and Bioinorganic Perspectives. *Chem. Rev.* **94**, 737–757 (1994).

51. Karlin, K. D., Hayes, J. C., Gultneh, Y., Cruse, R. W., McKown, J. W., Hutchinson, J. P. & Zubieta, J. Copper-Mediated Hydroxylation of an Arene: Model System for the Action of Copper Monooxygenases. Structures of a Binuclear Cu(I) Complex and Its Oxygenated Product. *J. Am. Chem. Soc.* **106**,

2121–2128 (1984).

52. Kaim, W. & Rall, J. Copper-A "Modern" Bioelement. *Angew. Chem. Int. Ed.* **35**, 43–60 (1996).

53. Fernandes, C., Neves, A., Bortoluzzi, A. J., Mangrich, A. S., Rentschler, E., Szpoganicz, B. & Schwingel, E. A new dinuclear unsymmetric copper(II) complex as model for the active site of catechol oxidase. *Inorganica Chim. Acta* **320**, 12–21 (2001).

54. Gentschev, P., Möller, N. & Krebs, B. New functional models for catechol oxidases. *Inorganica Chim. Acta* **300**–**302**, 442–452 (2000).

55. Ghosh, D., Lal, T. K. & Mukherjee, R. Dicopper complexes of relevance to tyrosinase modelling: An overview. *Proc. Indian Acad. Sci. Chem. Sci.* **108**, 251–256 (1996).

56. Rompel, A., Fischer, H., Biildt-karentzopoulos, K., Meiwes, D. & Zippel, F. Spectroscopic and EXAFS studies on Catechol Oxidases. **521**, 1994 (1994).

57. Rey, N. A., Neves, A., Bortoluzzi, A. J., Pich, C. T. & Terenzi, H. Catalytic promiscuity in biomimetic systems: Catecholase-like activity, phosphatase-like activity, and hydrolytic DNA cleavage promoted by a new dicopper(II) hydroxo-bridged complex. *Inorg. Chem.* **46**, 348–350 (2007).

58. Gerdemann, C., Eicken, C. & Krebs, B. The crystal structure of catechol oxidase: New insight into the function of type-3 copper proteins. *Acc. Chem. Res.* **35**, 183–191 (2002).

59. Becker, M., Schindler, S., Karlin, K. D., Kaden, T. A., Kaderli, S., Palanché, T. & Zuberbühler, A. D. Intramolecular ligand hydroxylation: Mechanistic high-pressure studies on the reaction of a dinuclear copper(I) complex with dioxygen. *Inorg. Chem.* **38**, 1989–1995 (1999).

60. Salunke, P. S., Puranik, A. A. & Kulkarni, N. D. Histamine derived dimer of μ-Chlorido-μ-Phenoxido Dicopper(II) complex as a potential enzyme mimic with catecholase activity. *Polyhedron* **216**, 115700 (2022).

•